iScience

CellPress
OPEN ACCESS

Article

Differential effects of bariatric surgery and caloric restriction on hepatic one-carbon and fatty acid metabolism

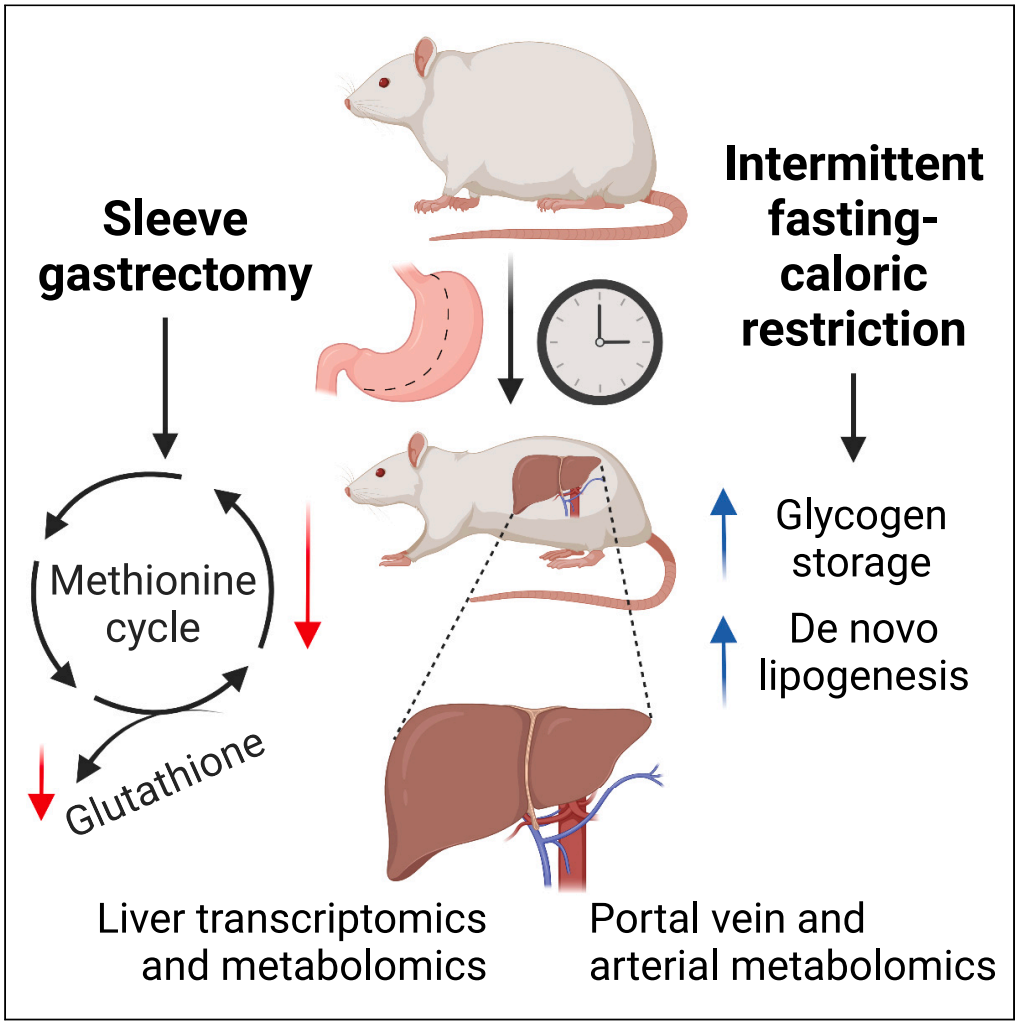

Arnon Haran, Michael Bergel, Doron Kleiman, ..., Rachel Ben-Haroush Schyr, Eyal Gottlieb, Danny Ben-Zvi

arnon@hadassah.org.il (A.H.)
danny.ben-zvi@mail.huji.ac.il (D.B.-Z.)

Highlights

Hepatic metabolism is affected differently by different weight loss interventions

Intermittent fasting results in increased lipogenesis and affects multiple pathways

Bariatric surgery uniquely affects one-carbon metabolic pathways and hepatic redox

Transmethylation cycle may be a promising target for treatment of metabolic disease

Haran et al., iScience 26, 107046
July 21, 2023
https://doi.org/10.1016/j.isci.2023.107046

iScience

CellPress
OPEN ACCESS

Article

Differential effects of bariatric surgery and caloric restriction on hepatic one-carbon and fatty acid metabolism

Arnon Haran,[1,5,*] Michael Bergel,[2] Doron Kleiman,[2] Liron Hefetz,[2] Hadar Israeli,[2] Sarah Weksler-Zangen,[3] Bella Agranovich,[4] Ifat Abramovich,[4] Rachel Ben-Haroush Schyr,[2] Eyal Gottlieb,[4] and Danny Ben-Zvi[2,*]

SUMMARY

Weight loss interventions, including dietary changes, pharmacotherapy, or bariatric surgery, prevent many of the adverse consequences of obesity, and may also confer intervention-specific benefits beyond those seen with decreased weight alone. We compared the molecular effects of different interventions on liver metabolism to understand the mechanisms underlying these benefits. Male rats on a high-fat, high-sucrose diet underwent sleeve gastrectomy (SG) or intermittent fasting with caloric restriction (IF-CR), achieving equivalent weight loss. The interventions were compared to *ad-libitum* (AL)-fed controls. Analysis of liver and blood metabolome and transcriptome revealed distinct and sometimes contrasting metabolic effects between the two interventions. SG primarily influenced one-carbon metabolic pathways, whereas IF-CR increased *de novo* lipogenesis and glycogen storage. These findings suggest that the unique metabolic pathways affected by SG and IF-CR contribute to their distinct clinical benefits, with bariatric surgery potentially influencing long-lasting changes through its effect on one-carbon metabolism.

INTRODUCTION

The worldwide prevalence of obesity is steadily increasing. In 2015, an estimated 12% of adults and 5% of children worldwide had obesity. Excess body weight accounted for about 4 million deaths and 120 million disability-adjusted life-years, most of these because of cardiovascular disease and diabetes.[1] Weight loss can prevent many of the adverse consequences of obesity, and can be achieved through either dietary and lifestyle interventions, pharmacotherapy, or bariatric surgery.[2] Some of these interventions have been purported to have benefits beyond those conferred by weight loss alone. For example, with regards to mortality and cardiovascular adverse events, the benefits of bariatric surgery were evident even with minimal weight loss, and greater degrees of weight loss were required to achieve the same effects through dietary intervention alone.[3,4] Likewise, an intermittent fasting (IF) regimen resulted in improved insulin sensitivity when compared to a similar degree of weight loss achieved through continuous energy restriction diets, both in humans and in animal models,[5–7] in addition to reported benefits for unrelated morbidities such as autoimmune disease, inflammatory disorders, and cancer.[8–11] The mechanisms underlying these beneficial effects remain largely unknown. Numerous unique metabolic alterations have been described with both bariatric surgery and IF. These include changes in serum amino acid and bile acid concentrations,[12,13] in the composition of the gut microbiome,[14,15] and in intestinal lipid handling.[16] The clinical significance of some of these alterations remains unclear.[17,18] We and others have previously demonstrated a specific and weight loss-independent effect of surgery on hepatic insulin sensitivity,[19–21] suggesting that changes in liver metabolism may explain some of the positive effects of surgery. Some effect of bariatric surgery on hepatic one-carbon metabolism, although not well characterized, has been identified in several human and animal studies.[22–25]

As the central organ for fatty acid (FA) metabolism,[26] the liver is also one of the primary organs affected by obesity. Excessive weight is often associated with an alteration of hepatic FA metabolism in which the liver's capacity to handle FAs and other metabolic energy substrates is overwhelmed,[27] leading to an accumulation of lipids within hepatocytes, a condition known as non-alcoholic fatty liver (NAFL) or hepatic steatosis.[28,29] In the present work, we seek to describe the changes in hepatic metabolic metabolism brought

[1]Department of Hematology, Haddasah Medical Center, Jerusalem, Israel

[2]Department of Developmental Biology and Cancer Research, Institute for Medical Research Israel-Canada, The Hebrew University of Jerusalem-Hadassah Medical School, Jerusalem, Israel

[3]The Hadassah Diabetes Center, Haddasah Medical Center, Jerusalem, Israel

[4]Department of Cell Biology and Cancer Science, Rappaport Faculty of Medicine, Technion - Israel Institute of Technology, Haifa, Israel

[5]Lead contact

*Correspondence: arnon@hadassah.org.il (A.H.), danny.ben-zvi@mail.huji.ac.il (D.B.-Z.)

https://doi.org/10.1016/j.isci.2023.107046

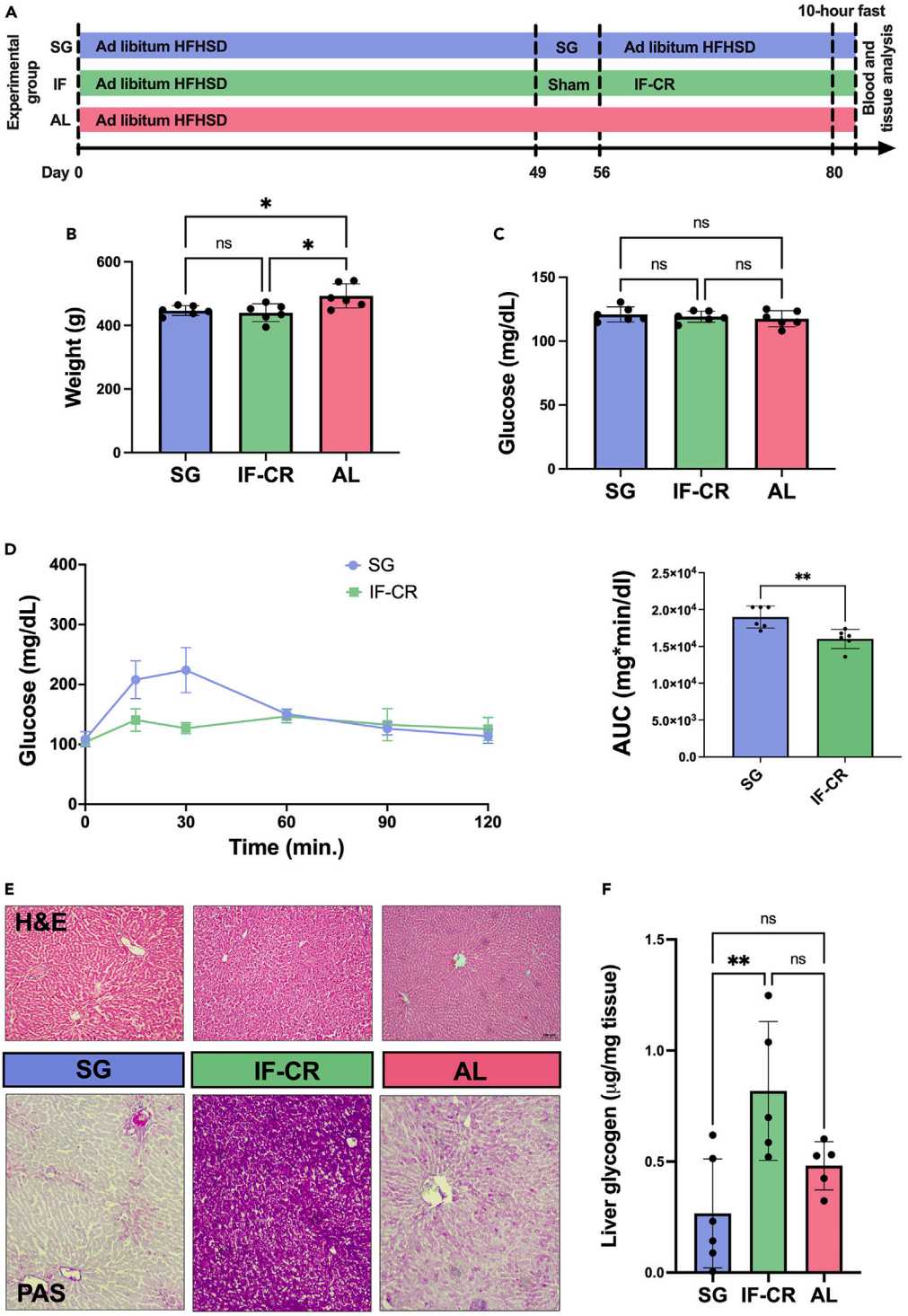

Figure 1. Overview and liver histology

(A) Experimental design. Animals were fed a high-fat, high-sucrose diet (HFHSD) for 7 weeks, and then underwent either sleeve gastrectomy (SG), sham surgery followed by intermittent fasting and caloric restriction (IF-CR), or no intervention (AL). At day 80, animals were sacrificed following a 10-h fast, and blood and tissue collected for analysis.

(B) Body weight of animals in the 3 experimental groups (mean ± SD).

(C) Morning non-fasting serum glucose measurements carried out in the three experimental groups.

Figure 1. *Continued*
(D) Oral glucose tolerance tests carried out at week 10 in the SG and IF-CR groups (mean ± SD). Left: Glucose measurements at five time points following oral gavage. Right: area under the curve (AUC; mean ± SD).
(E) Top: hematoxylin and eosin-stained liver sections, 10X magnification. Bottom: periodic acid-Schiff-stained liver sections, 10X magnification.
(F) Glycogen content in liver homogenates (mean ± SD).
*p < 0.05; **p < 0.01 (ANOVA with Tukey post-hoc test).

about by weight loss, and whether different interventions differ in this regard. We analyzed the metabolome of the hepatic blood supply and the metabolome and transcriptome of the liver itself following sleeve gastrectomy (SG), a common bariatric surgery, and IF with caloric restriction (IF-CR), in rats fed a high-fat, high-sucrose diet (HFHSD). Both interventions, when compared to *ad libitum* (AL)-fed animals, led to a similar loss of weight but resulted in distinct and in some cases contradictory effects on several metabolic pathways, when compared to an ad libitum-fed control group. The effect of bariatric surgery is apparent chiefly within pathways related to methionine and methyl group metabolism. In contrast, IF-CR has a profound effect on fatty acid metabolism and synthesis, which remain relatively unaffected by SG, as compared to *ad-libitum* fed rats.

RESULTS

At the conclusion of 12 weeks of HFHSD, animals attained an average weight of 456.3 g (+/− 14.4 g) in the SG group, 464.7 g (+/− 26.6 g) in the IF-CR group, and 492.8 g (+/−39.2 g) in the AL group (Figure 1B). Morning non-fasting serum glucose levels were unaltered between the experimental groups (Figure 1C). Following oral glucose loading, the IF-CR group showed improved glucose tolerance when compared to the SG group (Figure 1D), as manifested in a decreased glucose area under the curve.

Livers were examined histologically, which revealed a relative abundance of glycogen in the IF-CR group (Figure 1E). Other than this finding, which was corroborated by a biochemical glycogen assay (Figure 1F), there were no significant differences in liver histology, which appeared normal.

Metabolomic analysis of serum entering the liver

In analysis of the metabolic composition of the hepatic input, 87 of 197 metabolites were identified as altered between the experimental groups (Figures 2A–2C). PLS-DA showed separation of the IF-CR group from the SG and AL groups along the first component, and of the SG group from the two other groups primarily along the second component (Figure 2D). Pathway enrichment analysis showed component one to be enriched for fatty acid beta oxidation and biosynthesis, linolenic and linoleic acid metabolism, and ketone body metabolism (Figure 2E). Component two was enriched for glycine and serine metabolism (with relevant metabolites including methionine, betaine, creatine, glycine, guanidinoacetic acid, serine, glutamate, threonine, and alpha-ketoglutarate), glutathione metabolism, carnitine synthesis, and methionine metabolism (Figure 2F).

Within the differentially regulated metabolites in the hepatic input, several patterns of between-group differences were seen (Figure 2G, Table S1). One group of compounds was similarly affected by both SG and IF-CR. Levels of serum kynurenine, a tryptophan breakdown product, of serum creatine, and of glutathione and its precursors γ-glutamyl-cysteine and cystathionine, were all reduced in both weight loss intervention groups. In contrast, levels of the micronutrients thiamine and ascorbic acid (vitamins B1 and C), and of the amino acids methionine, threonine, and serine, were all lower in the AL-fed group.

Another group of metabolites was upregulated in the SG group and downregulated in the IF-CR group. Among these were numerous metabolites related to one-carbon metabolism and methyl transfer reactions, including betaine, dimethylglycine, sarcosine, and glycine. Other metabolites showing a similar pattern were the pyrimidine nucleotides (cytidine and thymidine) and the polyunsaturated ω-3 long-chain fatty acids (LCFAs).

Metabolites downregulated exclusively in the IF-CR group include the ketone bodies acetoacetate (AcAc) and beta-hydroxybutyrate (beta-HB) and certain saturated and mono-unsaturated LCFAs. Notable compounds upregulated with IF-CR include the gluconeogenic precursors alanine and glycerate, proline, the branched-chain amino acids valine, leucine, and isoleucine, and gut microbiota-derived metabolites, including short- and medium-chain free fatty acids (butyric, caproic, and caprylic acids), and the tryptophan

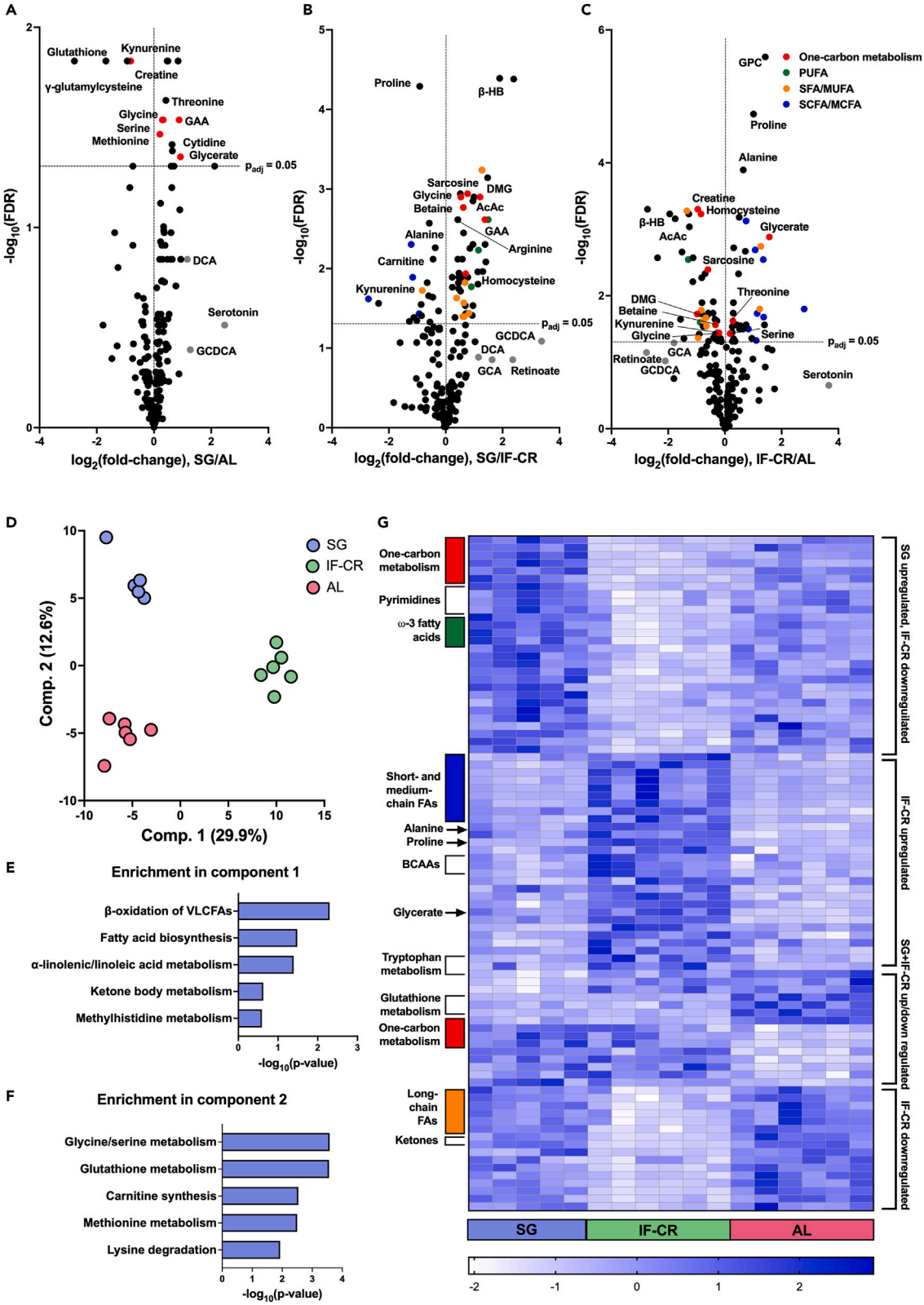
A
B
C
Glutathione
Kynurenine
Creatine
γ-glutamylcysteine
Threonine
Glycine
GAA
Serine
Methionine
Cytidine
Glycerate
p_{adj} = 0.05
DCA
Serotonin
GCDCA
-log10(FDR)
log2(fold-change), SG/AL
Proline
β-HB
Sarcosine
DMG
Glycine
Betaine
AcAc
GAA
Alanine
Arginine
Carnitine
Homocysteine
Kynurenine
p_{adj} = 0.05
GCDCA
DCA
GCA
Retinoate
log2(fold-change), SG/IF-CR
GPC
One-carbon metabolism
PUFA
SFA/MUFA
SCFA/MCFA
Proline
Alanine
Creatine
Homocysteine
β-HB
Glycerate
AcAc
Sarcosine
Threonine
DMG
Betaine
Kynurenine
Glycine
Serine
p_{adj} = 0.05
GCA
Retinoate
GCDCA
Serotonin
log2(fold-change), IF-CR/AL
D
SG
IF-CR
AL
Comp. 2 (12.6%)
Comp. 1 (29.9%)
E
Enrichment in component 1
β-oxidation of VLCFAs
Fatty acid biosynthesis
α-linolenic/linoleic acid metabolism
Ketone body metabolism
Methylhistidine metabolism
-log10(p-value)
F
Enrichment in component 2
Glycine/serine metabolism
Glutathione metabolism
Carnitine synthesis
Methionine metabolism
Lysine degradation
-log10(p-value)
G
One-carbon metabolism
Pyrimidines
ω-3 fatty acids
Short- and medium-chain FAs
Alanine
Proline
BCAAs
Glycerate
Tryptophan metabolism
Glutathione metabolism
One-carbon metabolism
Long-chain FAs
Ketones
SG upregulated, IF-CR downregulated
IF-CR upregulated
SG+IF-CR up/down regulated
IF-CR downregulated
SG
IF-CR
AL

Figure 2. Metabolomic analysis of blood entering the liver

(A–C) Volcano plots showing the relative changes in metabolite concentrations in the hepatic input (80% portal blood, 20% aortic blood) between the experimental groups (SG: sleeve gastrectomy; IF-CR: intermittent fasting caloric restriction; AL: *ad libitum*; FDR = false discovery rate-adjusted p value of between-group t-tests; PUFA: poly-unsaturated long-chain free fatty acids; SFA/MUFA: saturated/mono-unsaturated long-chain free fatty acids; SCFA/MCFA: short-/medium-chain free fatty acids).

(D) Partial least squares-discriminant analysis (PLS-DA) scores plot of metabolite abundance demonstrating separation of the IF-CR group from the AL group along the first component and of the SG group from the AL group along the second component.

(E and F) Enrichment analysis by small molecule pathway database (SBPDB) pathways of metabolites in components 1 (E) and 2 (F) of PLS-DA. Metabolites were defined as belonging to component one, two, or neither, based on their VIP score for that component being above 1.0 and greater than the VIP score for the other component.

(G) Heatmap of normalized concentrations of 87 metabolites identified as significantly altered between the experimental groups by ANOVA with FDR of <0.05.

breakdown product indole 3-acetate (IAA), which functions as a central mediator in gut microbiota-host interactions.[30,31]

Looking separately at each component of the hepatic input, i.e., aortic and portal blood, we find that the two can be readily distinguished by their metabolic composition (Figures 3A–3C). PLS-DA with separate analysis of each blood pool from the three experimental groups showed clear separation of the IF-CR group from the two other groups, as well as clear separation of aortic and portal blood. However, there was considerable overlap between aortic samples from the SG and AL groups, as well as between portal samples from these two groups (Figure 3D). Correlation analysis using data from all three experimental groups revealed several metabolites whose concentrations were either higher or lower in the portal versus aortic blood. Notably, ratios of metabolite concentrations between aortic and portal blood were consistent across the experimental groups, and no statistically significant differences were seen in these ratios for all metabolites examined, despite numerous between-group differences in absolute metabolite concentrations, as detailed above. Portal blood from all groups was characterized by higher concentrations of asparagine, arginine, histidine, alanine, glycine, and proline, and by lower concentrations of glucose, glutamine, and creatinine, when compared to aortic blood. Levels of choline and, predictably, bile salts, were also higher in the portal blood.

Metabolomic analysis of liver

In the liver itself, significant changes were seen in the concentrations of 51 of 241 metabolites across the experimental groups (Figures 4A–4C). PLS-DA showed separation of the IF-CR group from the SG and AL groups along the first component, and separation of the SG group from the two other groups along the second component (Figure 4D). Pathway enrichment showed component one to be enriched for glutamate metabolism, fatty acid and plasmalogen biosynthesis, purine metabolism, and carnitine synthesis. Component two was enriched for glycine and serine metabolism as well as glycolysis/gluconeogenesis and pentose phosphate pathway-related metabolites and ammonia recycling (Figures 4E and 4F).

As in the serum, several metabolites showed opposite trends in the SG and IF-CR groups when compared to the AL group (Figure 4G, Table S2). Compounds whose concentrations were increased in the SG groups and decreased in the IF-CR group included one-carbon metabolism-related metabolites and the biogenic amines serotonin and histamine. Showing an opposite pattern were glutathione and the phosphorylated sugars glucose and fructose 6-phosphate. Other metabolites were exclusively affected in the IF-CR group. Consistent with their plasma concentrations, alanine, proline, and isoleucine, and the short-chain free fatty acids (butyric and hexanoic acid), were all increased in the IF-CR group. In contrast, the LCFAs, the majority of which showed decreased serum concentrations in the IF-CR group, as mentioned above, were seen to be increased intrahepatically in this group in comparison to the two others.

Transcriptomic analysis of liver

2645 differentially expressed genes were identified, of which 1222 were upregulated and 819 were downregulated in the IF-CR group, while 636 were upregulated and 902 were downregulated in the SG group compared to the AL group (Figures 5A–5C). Genes upregulated in the IF-CR group were found to be enriched for citrate cycle, pyruvate metabolism, glycolysis/gluconeogenesis, pentose phosphate pathway, glycine, serine, and threonine metabolism, and fatty acid biosynthesis, whereas downregulated pathways included fatty acid degradation and linoleic acid metabolism (Figure 5D). For the SG group, prominent downregulated pathways were those of glycine, serine, and threonine metabolism, cysteine and methionine metabolism, citrate cycle, and pyruvate metabolism, whereas fatty acid degradation, linoleic acid

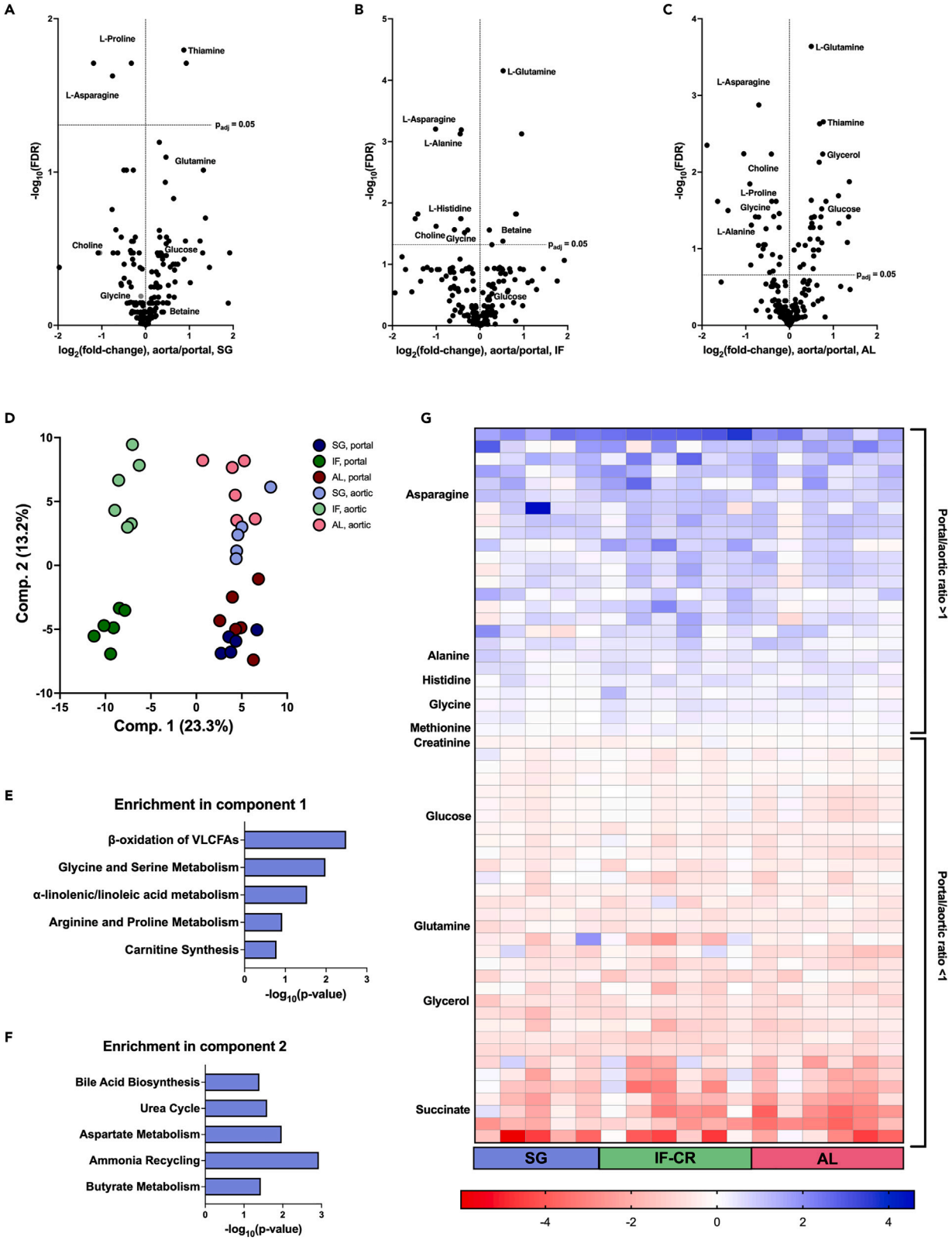
A
L-Proline
Thiamine
L-Asparagine
p_{adj} = 0.05
Glutamine
Choline
Glucose
Glycine
Betaine
-log10(FDR)
log2(fold-change), aorta/portal, SG
B
L-Glutamine
L-Asparagine
L-Alanine
L-Histidine
Choline
Glycine
Betaine
p_{adj} = 0.05
Glucose
-log10(FDR)
log2(fold-change), aorta/portal, IF
C
L-Glutamine
L-Asparagine
Thiamine
Glycerol
Choline
L-Proline
Glycine
Glucose
L-Alanine
p_{adj} = 0.05
-log10(FDR)
log2(fold-change), aorta/portal, AL
D
SG, portal
IF, portal
AL, portal
SG, aortic
IF, aortic
AL, aortic
Comp. 2 (13.2%)
Comp. 1 (23.3%)
E
Enrichment in component 1
β-oxidation of VLCFAs
Glycine and Serine Metabolism
α-linolenic/linoleic acid metabolism
Arginine and Proline Metabolism
Carnitine Synthesis
-log10(p-value)
F
Enrichment in component 2
Bile Acid Biosynthesis
Urea Cycle
Aspartate Metabolism
Ammonia Recycling
Butyrate Metabolism
-log10(p-value)
G
Asparagine
Alanine
Histidine
Glycine
Methionine
Creatinine
Glucose
Glutamine
Glycerol
Succinate
Portal/aortic ratio >1
Portal/aortic ratio <1
SG
IF-CR
AL

Figure 3. Metabolomic comparison of aortic and portal blood

(A–C) Volcano plots showing the relative concentrations of metabolites in aortic vs. portal blood in each experimental gorup (SG: sleeve gastrectomy; IF-CR: intermittent fasting caloric restriction; AL: *ad libitum*; FDR = false discovery rate-adjusted p value of between-group t-tests).

(D) Partial least squares-discriminant analysis (PLS-DA) scores plot of metabolite abundance demonstrating separation of the IF-CR group from the AL group along the first component and of aortic from portal samples along the second component.

(E and F) Enrichment analysis by small molecule pathway database (SBPDB) pathways of metabolites in components 1 (E) and 2 (F) of PLS-DA. Metabolites were defined as belonging to component one, two, or neither, based on their VIP score for that component being above 1.0 and greater than the VIP score for the other component.

(G) Heatmap of the log2(portal to aortic ratio) of 58 metabolites identified as significantly correlated with aortic or portal source across experimental groups (FDR <0.1).

metabolism, and tryptophan and nicotinamide metabolism were upregulated (Figure 5E). PCA showed distinct separation of the IF-CR group from the two other groups along the first principal component, and lesser separation of the SG group from both other groups along the second principal component (Figure 5F). A joint pathway analysis incorporating both significantly altered metabolites and genes (Figure 5G) showed glycolysis/gluconeogenesis, citric acid cycle, and pyruvate metabolism to be significantly altered in the IF-CR compared to the AL group, and glycine, serine, and threonine metabolism and cysteine and methionine metabolism as significantly altered in the SG compared to the AL group.

One-carbon metabolism: Decreased utilization of one-carbon donors following SG

Transfer of methyl groups is centered around the transmethylation cycle, which involves conversion of methionine to S-adenosylmethionine (SAM), the universal methyl donor, and then to homocysteine. Methionine is then regenerated in a reaction utilizing either betaine or tetrahydrofolate as the source of a one-carbon unit. As described above, the most prominent effects of SG were seen in metabolites and transcripts related to one-carbon metabolic pathways. Levels of the major one-carbon donors, including betaine, methionine, serine, glycine, sarcosine, and dimethylglycine (DMG), were increased in both the serum and intrahepatically. With IF-CR, decreased levels of betaine, DMG, sarcosine, and glycine, which are intermediates in the sequential breakdown of choline to glycine, were seen in the serum (Figure 6A). Levels of methyl-utilizing enzymes involved in the transfer of one-carbon groups for regeneration of SAM, including betaine homocysteine S-methyltransferase (*BHMT*), dimethylglycine dehydrogenase (*DMGDH*), mitochondrial serine hydroxymethyltransferase (*SHMT2*), and glycine decarboxylase (*GLDC*), were all decreased in the SG group compared to the AL and IF-CR group (Figure 6B), suggesting that reduced consumption of one-carbon groups through the transmethylation cycle underlies the observed increase in potential methyl donors.

Levels of SAM and SAM/S-adenosylhomocysteine (SAH) ratios were not significantly altered between the experimental groups (Figure 6C). However, changes in the ratios of methylated products to their unmethylated precursors could account for the apparent changes in methyl donor utilization. Conversion of the phospholipid phosphoethanolamine (PE) to phosphatidylcholine (PC), and the methylation of guanidinoacetic acid (GAA) to form creatine, are the two major methyl-consuming reactions in the liver and the body as a whole.[32,33] The ratio of creatine to GAA was reduced post-SG when compared to both other groups. In contrast, the intrahepatic PC/PE ratio was increased in the IF-CR group (Figure 6C). Levels of choline kinase (*CHKA*), which catalyzes the rate-limiting step in the synthesis of PC from choline (Kennedy pathway), were reduced post-SG (Figure 6F), suggesting that the apparent reduced consumption of methyl groups is not because of increased synthesis of PC via this pathway. Levels of *ABCB4/MDR3*, which is responsible for secretion of PC into bile,[34] were decreased in both the SG and IF-CR groups when compared to the AL group.

Redox balance: Decreased hepatic glutathione concentrations following SG

Homocysteine generated in the transmethylation cycle serves as a precursor for the synthesis of glutathione, the major hepatic antioxidant. Consistent with decreased transmethylation activity, we found decreased levels of glutathione in the post-SG livers, as well as a decreased ratio of reduced to oxidized glutathione (GSH/GSSG; Figure 6D). This finding contrasts with an increased expression of subunits of the rate-limiting enzyme in GSH biosynthesis, glutamate-cysteine ligase (*GCLC* and *GCLM*; Figure 6F), suggesting upstream substrate availability as the cause of decreased GSH post-SG. Additional evidence for a more oxidized metabolic state post-surgery was seen with an increased ratio of AcAc to beta-HB, which provides an estimate of the mitochondrial ratio of oxidized to reduced nicotinamide adenine dinucleotide (NAD+/NADH),[35] as well as an increase in the ratios of pyruvate to malate and lactate, which provide an estimate of the cytosolic ratios of oxidized to reduced nicotinamide adenine dinucleotide phosphate (NADP+/NADPH) and NAD+/NADH, respectively (Figure 6E). This effect was particularly prominent in comparing the SG to the AL group, and

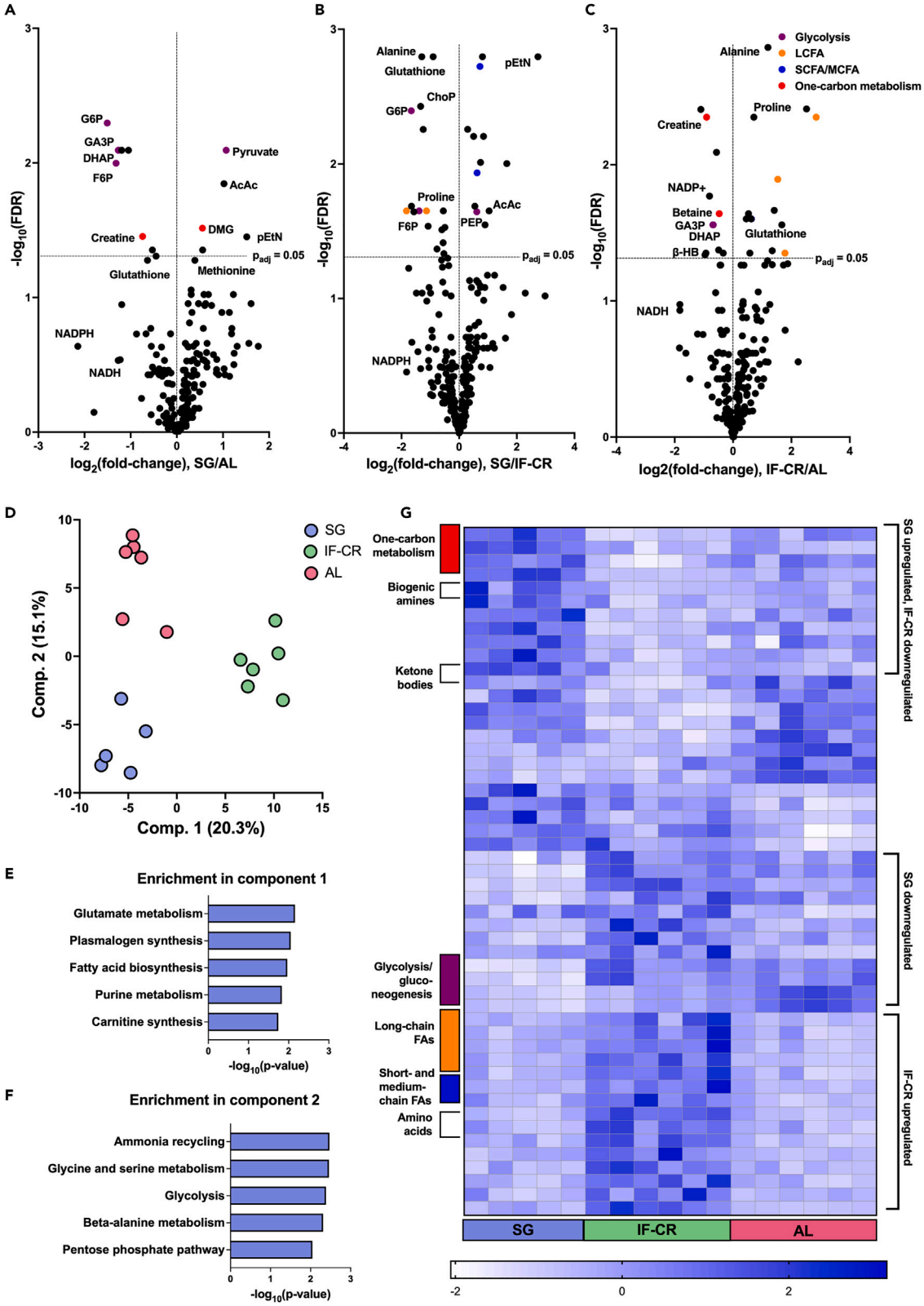
A
B
C
G6P
GA3P
DHAP
F6P
Pyruvate
AcAc
DMG
pEtN
Creatine
Glutathione
Methionine
NADPH
NADH
Alanine
ChoP
Proline
PEP
Glycolysis
LCFA
SCFA/MCFA
One-carbon metabolism
NADP+
Betaine
β-HB
-log10(FDR)
padj = 0.05
log2(fold-change), SG/AL
log2(fold-change), SG/IF-CR
log2(fold-change), IF-CR/AL
D
SG
IF-CR
AL
Comp. 2 (15.1%)
Comp. 1 (20.3%)
E
Enrichment in component 1
Glutamate metabolism
Plasmalogen synthesis
Fatty acid biosynthesis
Purine metabolism
Carnitine synthesis
-log10(p-value)
F
Enrichment in component 2
Ammonia recycling
Glycine and serine metabolism
Glycolysis
Beta-alanine metabolism
Pentose phosphate pathway
G
One-carbon metabolism
Biogenic amines
Ketone bodies
Glycolysis/ gluco-neogenesis
Long-chain FAs
Short- and medium-chain FAs
Amino acids
SG upregulated, IF-CR downregulated
SG downregulated
IF-CR upregulated
SG
IF-CR
AL

Figure 4. Metabolomic analysis of liver

(A–C) Volcano plots showing the relative changes in metabolite concentrations in the liver between the experimental groups (SG: sleeve gastrectomy; IF-CR: intermittent fasting caloric restriction; AL: *ad libitum*; FDR = false discovery rate-adjusted p value of between-group t-tests; LCFA: long-chain free fatty acids; SCFA/MCFA: short-/medium-chain free fatty acids).

(D) Partial least squares-discriminant analysis (PLS-DA) scores plot of metabolite abundance demonstrating separation of the IF-CR group from the AL group along the first component and of the SG group from the AL group along the second component.

(E and F) Enrichment analysis by small molecule pathway database (SBPDB) pathways of metabolites in components 1 (E) and 2 (F) of PLS-DA. Metabolites were defined as belonging to component one, two, or neither, based on their VIP score for that component being above 1.0 and greater than the VIP score for the other component.

(G) Heatmap of normalized concentrations of 51 metabolites identified as significantly altered between the experimental groups by ANOVA with FDR of <0.05.

less so with respect to the IF-CR group. Increased glutathione oxidation is linked to attenuated endoplasmic reticulum (ER) stress,[36] and we found decreased expression of unfolded protein response genes (*HSPA5/BIP*, *EIF2AK3/PERK*), which are markers of ER stress, in the SG group (Figure 6F). The changes in one-carbon and redox pathways following SG are summarized in Figure 6G.

Fatty acid metabolism: Lipogenic pathways increased by IF-CR

SG had little effect on lipid metabolism, with the exception of an increase in the transcript levels of key enzymes of fatty acid beta-oxidation, including carnitine palmitoyl transferase 1 (*CPT1*) and acyl-CoA oxidase 1 (*ACOX1*), which catalyze the rate-limiting steps in mitochondrial and peroxisomal β-oxidation, respectively.[37,38] Both enzymes were upregulated by approximately 2-fold in the SG group when compared to the AL-fed animals. In contrast, these two enzymes were downregulated in the IF-CR group when compared to the AL group, in addition to numerous other changes relating to lipid metabolism. We witnessed in the IF-CR group a decreased concentration of long-chain FAs (LCFAs) in blood entering the liver but an increased concentration of intrahepatic LCFAs (Figure 7A) when compared to both the SG and AL groups. An almost 3-fold increase in serum triglycerides (TGs) was seen in the IF-CR group in comparison to the SG group (Figure 7B), as well as a decrease in serum ketone bodies (AcAc and beta-HB, Figure 7C). These changes were paralleled by a dramatic increase in the expression of enzymes involved in *de novo* lipogenesis (DNL) and in TG mobilization within the liver in the IF-CR group. In particular, the expression of rate-limiting enzymes of DNL, acetyl-CoA carboxylase (*ACACA*), fatty acid synthetase (*FASN*), acetyl-CoA citrate lyase (*ACLY*), and stearoyl-CoA desaturase (*SCD*),[39] was increased between 8- and 50-fold in the IF-CR group compared to the AL group (Figure 7D).

In parallel with an increase in fatty acid synthetic pathways, we observed in the IF-CR group an increased expression of glycolytic, pentose phosphate pathway, and citrate cycle enzymes (Figure 5E), and increased levels of glycolytic intermediates in the liver (Figure 7F). The changes related to fatty acid metabolism following IF-CR are summarized in Figure 7G.

DISCUSSION

In this study, we sought to compare the changes in liver metabolism following weight loss induced by either SG or IF-CR in a rat model, using combined metabolomic and transcriptomic approaches. We chose an experimental design in which animals were fed a moderately high-fat high-sucrose diet for a relatively short period. This design was meant to examine the effects of SG and IF-CR but separated from the metabolic disturbances wrought by frank liver steatosis or the development of impaired glucose tolerance seen with prolonged high-fat feeding. Thus, both interventions resulted in significant, though modest, weight loss when compared to AL-fed animals.

Importantly, each of the interventions had a distinct effect on hepatic metabolism. The metabolic changes following SG concentrated primarily on one-carbon metabolic pathways. The levels of most major methyl donors in the blood entering the liver were increased post-SG. The levels of methyl acceptors were either markedly increased, as in the case of GAA, the precursor to creatine, or unchanged, e.g., in the case of PE and PC. Contrasting with the increase in these substrates, quantities of transcripts encoding for key enzymes within the transmethylation cycle were decreased. Levels of glutathione, generated downstream of the transmethylation cycle, were also reduced.

The increased levels of both methyl donors and methyl acceptors suggest altered regulation at the entry point of the transmethylation cycle. Decreased glutathione and decreased allocation of methyl groups to

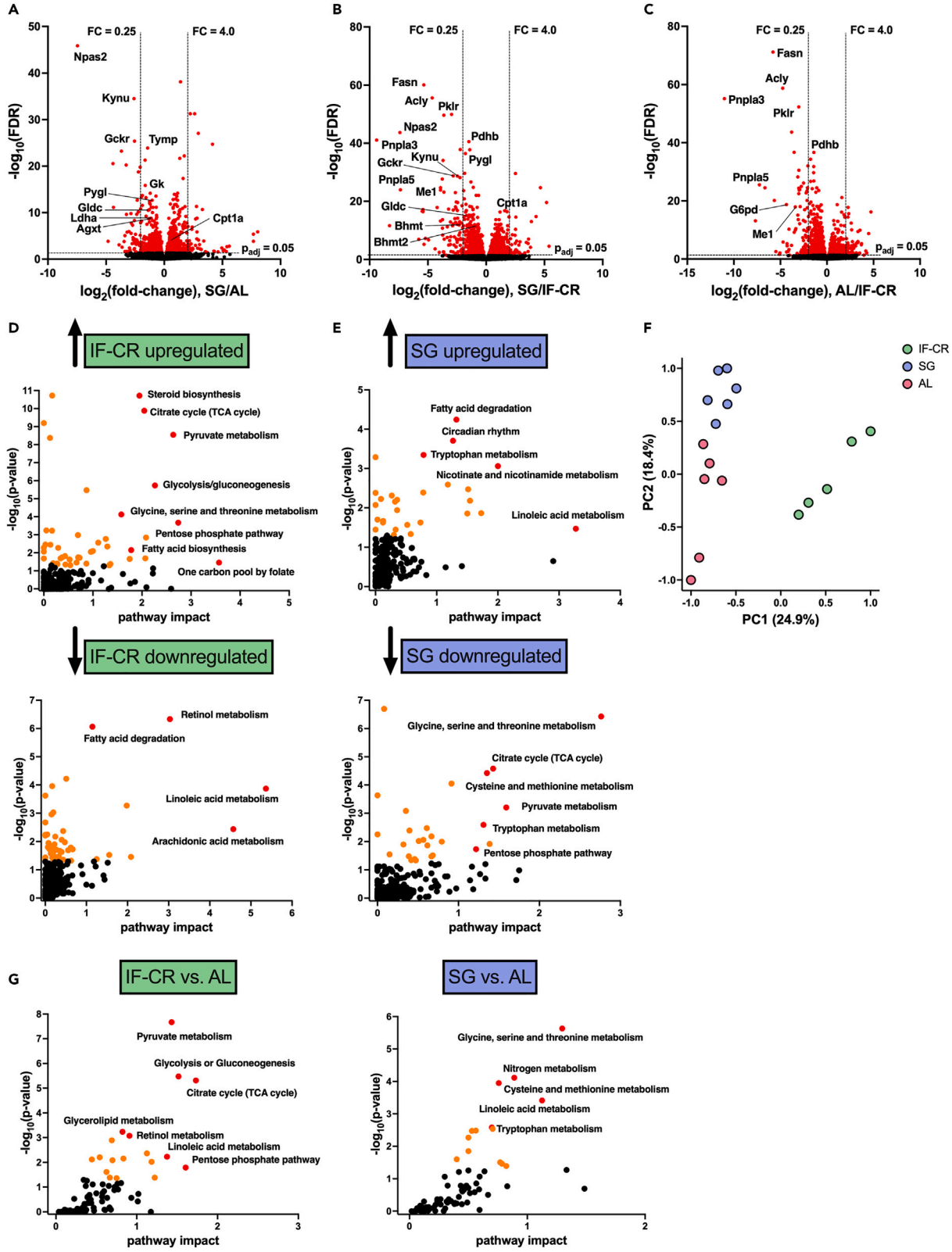
A
FC = 0.25
FC = 4.0
Npas2
Kynu
Gckr
Tymp
Gk
Pygl
Gldc
Ldha
Agxt
Cpt1a
p_{adj} = 0.05
$-\log_{10}$(FDR)
$\log_2$(fold-change), SG/AL
B
FC = 0.25
FC = 4.0
Fasn
Acly
Pklr
Npas2
Pdhb
Pnpla3
Kynu
Gckr
Pygl
Pnpla5
Me1
Gldc
Cpt1a
Bhmt
Bhmt2
p_{adj} = 0.05
$-\log_{10}$(FDR)
$\log_2$(fold-change), SG/IF-CR
C
FC = 0.25
FC = 4.0
Fasn
Acly
Pnpla3
Pklr
Pdhb
Pnpla5
G6pd
Me1
p_{adj} = 0.05
$-\log_{10}$(FDR)
$\log_2$(fold-change), AL/IF-CR
D
IF-CR upregulated
Steroid biosynthesis
Citrate cycle (TCA cycle)
Pyruvate metabolism
Glycolysis/gluconeogenesis
Glycine, serine and threonine metabolism
Pentose phosphate pathway
Fatty acid biosynthesis
One carbon pool by folate
$-\log_{10}$(p-value)
pathway impact
IF-CR downregulated
Retinol metabolism
Fatty acid degradation
Linoleic acid metabolism
Arachidonic acid metabolism
$-\log_{10}$(p-value)
pathway impact
E
SG upregulated
Fatty acid degradation
Circadian rhythm
Tryptophan metabolism
Nicotinate and nicotinamide metabolism
Linoleic acid metabolism
$-\log_{10}$(p-value)
pathway impact
SG downregulated
Glycine, serine and threonine metabolism
Citrate cycle (TCA cycle)
Cysteine and methionine metabolism
Pyruvate metabolism
Tryptophan metabolism
Pentose phosphate pathway
$-\log_{10}$(p-value)
pathway impact
F
IF-CR
SG
AL
PC2 (18.4%)
PC1 (24.9%)
G
IF-CR vs. AL
Pyruvate metabolism
Glycolysis or Gluconeogenesis
Citrate cycle (TCA cycle)
Glycerolipid metabolism
Retinol metabolism
Linoleic acid metabolism
Pentose phosphate pathway
$-\log_{10}$(p-value)
pathway impact
SG vs. AL
Glycine, serine and threonine metabolism
Nitrogen metabolism
Cysteine and methionine metabolism
Linoleic acid metabolism
Tryptophan metabolism
$-\log_{10}$(p-value)
pathway impact

Figure 5. Transcriptomic analysis of liver

(A–C) Volcano plots showing the relative changes in transcript abundance in the liver between the experimental groups (SG: sleeve gastrectomy; IF-CR: intermittent fasting caloric restriction; AL: *ad libitum*; FDR = false discovery rate-adjusted p value of between-group t-tests). Red denotes differentially expressed transcripts.

(D and E) Enrichment analysis by Kyoto Encyclopedia of Genes and Genomes (KEGG) pathways of genes identified as upregulated (top) or downregulated (bottom) in the IF-CR (D) and SG (E) groups; genes were defined as up- or down-regulated if identified by ANOVA (FDR <0.05) and post-hoc analysis as significantly altered against at least one of the other experimental groups, and with either a negative or positive fold-change compared to both other groups.

(F) Principal component analysis (PCA) scores plot of transcript abundance demonstrating separation of the IF-CR group from the AL group along the first component and of the SG group from the AL group along the second component.

(G) Joint pathway enrichment analysis by KEGG pathways of genes and metabolites identified as significantly altered by ANOVA (FDR <0.05) and post-hoc analysis between the IF-CR and AL groups (left) and between the SG and AL groups (right).

creatine synthesis are features commonly observed in methionine restricted diets.[40–43] Despite an abundance of methionine and other methyl donors, these features were seen in our study post-SG. Methionine adenosyltransferase 1A (MAT1A) catalyzes the entry of methionine into the transmethylation cycle. Levels of MAT1A mRNA were not altered post-SG; nevertheless, the metabolic profile established post-SG is similar to that described with specific downregulation of MAT1A.[44] The activity of this enzyme is modulated post-transcriptionally by reactive oxygen species, glutathione, and nitric oxide (NO),[45–48] through oxidation or nitrosylation of a specific cysteine residue. Levels of NO are increased following bariatric surgery,[49,50] an effect perhaps mediated by increased GLP-1-signalling.[51,52] Thus, changes in either NO metabolism or hepatic redox status post-SG may explain the change in transmethylation activity.

One-carbon metabolism is central to many cellular processes, including phospholipid metabolism, creatine synthesis, nucleotide synthesis, maintenance of DNA, RNA, and protein methylation, and, as noted above, redox metabolism. An intriguing option, to be probed in future studies, is that the epigenetic changes observed following bariatric surgery[53] are driven at least partly by decreased transmethylation. However, changes in hepatic redox metabolism may have a more direct effect. Although oxidative stress is generally thought of as a deleterious phenomenon, the early stages of the development of liver steatosis are characterized by *increased* antioxidant capacity and GSH synthesis,[54,55] and several studies have pointed to a beneficial effect of reactive oxygen species (ROS) generation and glutathione depletion early in the development of NAFL[36,44,56–58] or in the context of a methionine- and choline-deficient diet.[58] Indeed, an anti-obesity effect of MAT1A downregulation was found to be mediated by a decrease in glutathione production.[44] Intriguingly, as noted above, decreased glutathione may itself lead to a decrease in MAT1A activity, resulting in a feedback mechanism which stabilizes this new metabolic state. A decrease in antioxidant capacity may underlie both the beneficial effect in the majority of patients, and the puzzling worsening of NAFL features in a subset (approximately 10%) of patients undergoing bariatric surgery,[59] as well the increased susceptibility to acetaminophen toxicity which has been reported in several human studies.[60–62]

Beyond effects on the liver itself, alterations in hepatic one-carbon metabolism may have profound systemic consequences. The liver is the major consumer of methyl groups in the body. Therefore, alterations in hepatic methyl group utilization may affect the availability of one-carbon groups in other organs. Dietary intake of methionine influences immune responses through an effect on T cell activation, mediated by SAM availability.[63,64] Thus, an increase in one-carbon donors following surgery may in part mediate both beneficial and deleterious effects on the immune system seen following this intervention.[65] For example, a negative effect on the clinical course of multiple sclerosis is described following bariatric surgery,[66] whereas methionine restriction was found to have a positive effect on this disease in pre-clinical models.[63] Likewise, SG was found to result in altered anti-cancer immunity, with a dampened anti-tumor immune response compared to weight-matched controls, but improved response to immune checkpoint blockade.[11]

Levels of glycine have been consistently observed to be lower in individuals with obesity and the metabolic syndrome, and to increase following bariatric surgery.[67] Our findings, showing higher glycine levels in the portal compared to the aortic blood pool, and decreased expression of glycine catabolic enzymes in the liver, suggest that decreased hepatic glycine consumption, reflecting a decreased demand for methyl donors, underlies the increased circulating glycine levels following bariatric surgery. Other explanations for this phenomenon have also been proposed.[68]

Although high-fat diets and the development of obesity have been shown to result in depletion of methyl donors,[69] the changes observed in one-carbon metabolism post-SG cannot be attributed to either loss

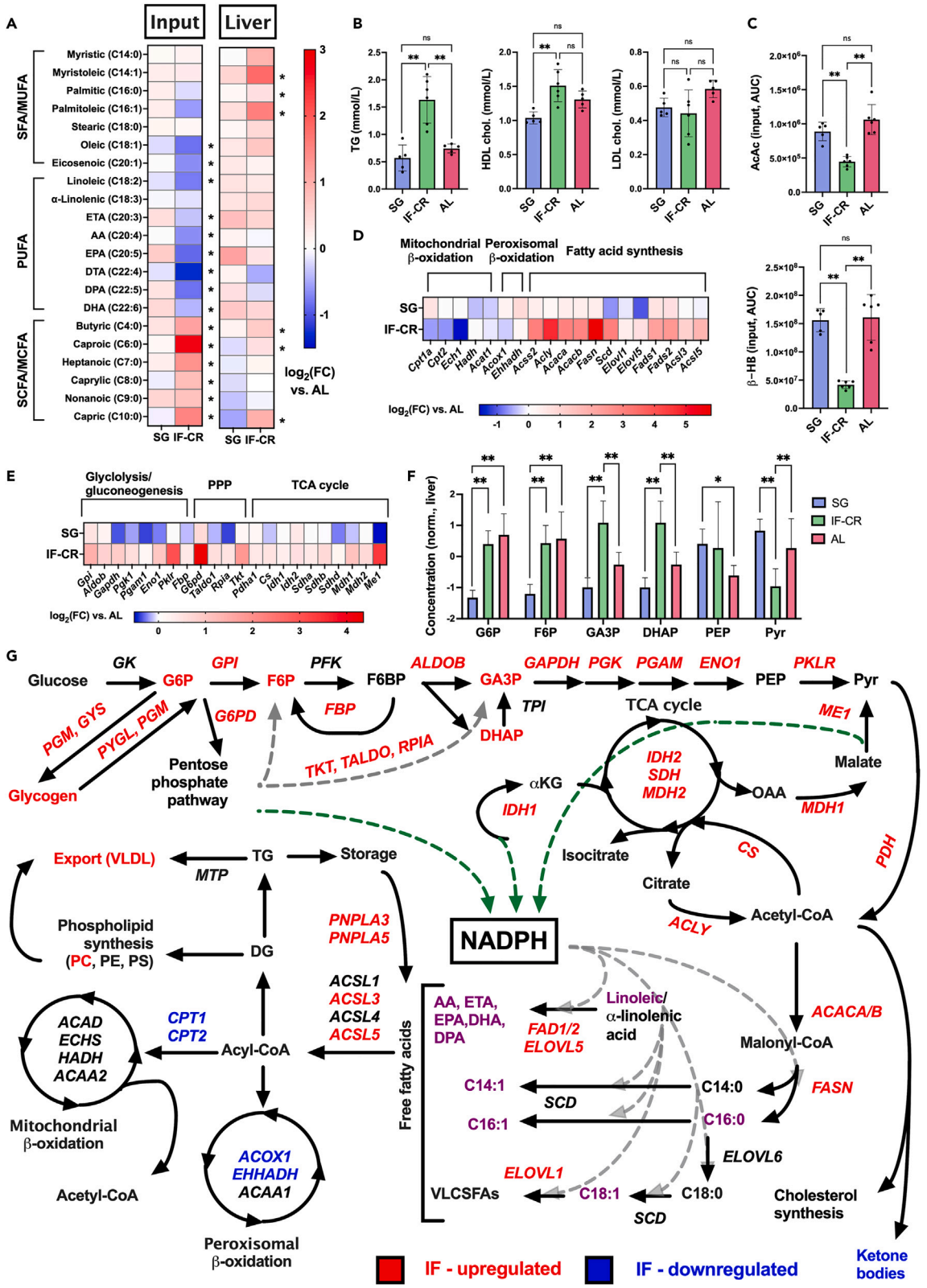
A
Input
Liver
SFA/MUFA
PUFA
SCFA/MCFA
Myristic (C14:0)
Myristoleic (C14:1)
Palmitic (C16:0)
Palmitoleic (C16:1)
Stearic (C18:0)
Oleic (C18:1)
Eicosenoic (C20:1)
Linoleic (C18:2)
α-Linolenic (C18:3)
ETA (C20:3)
AA (C20:4)
EPA (C20:5)
DTA (C22:4)
DPA (C22:5)
DHA (C22:6)
Butyric (C4:0)
Caproic (C6:0)
Heptanoic (C7:0)
Caprylic (C8:0)
Nonanoic (C9:0)
Capric (C10:0)
SG IF-CR
SG IF-CR
log2(FC) vs. AL
B
TG (mmol/L)
HDL chol. (mmol/L)
LDL chol. (mmol/L)
SG
IF-CR
AL
C
AcAc (input, AUC)
β−HB (input, AUC)
D
Mitochondrial β-oxidation
Peroxisomal β-oxidation
Fatty acid synthesis
SG
IF-CR
Cpt1a Cpt2 Ech1 Hadh Acat1 Acox1 Ehhadh Acss2 Acly Acaca Acacb Fasn Scd Elovl1 Elovl5 Fads1 Fads2 Acsl3 Acsl5
log2(FC) vs. AL
E
Glycolysis/ gluconeogenesis
PPP
TCA cycle
SG
IF-CR
Gpi Aldob Gapdh Pgk1 Pgam1 Eno1 Pklr Fbp G6pd Taldo1 Rpia Tkt Pdha1 Cs Idh1 Idh2 Sdha Sdhb Sdhd Mdh1 Mdh2 Me1
log2(FC) vs. AL
F
Concentration (norm., liver)
SG
IF-CR
AL
G6P F6P GA3P DHAP PEP Pyr
G
Glucose
GK
G6P
GPI
F6P
PFK
F6BP
ALDOB
GA3P
GAPDH PGK PGAM ENO1
PEP
PKLR
Pyr
PGM, GYS
PYGL, PGM
Glycogen
G6PD
FBP
TPI
DHAP
TKT, TALDO, RPIA
Pentose phosphate pathway
TCA cycle
ME1
Malate
IDH2 SDH MDH2
OAA
MDH1
αKG
IDH1
Isocitrate
CS
Citrate
PDH
Acetyl-CoA
ACLY
Export (VLDL)
MTP
TG
Storage
Phospholipid synthesis (PC, PE, PS)
DG
PNPLA3 PNPLA5
NADPH
ACSL1 ACSL3 ACSL4 ACSL5
AA, ETA, EPA,DHA, DPA
FAD1/2 ELOVL5
Linoleic/ α-linolenic acid
ACACA/B
Malonyl-CoA
FASN
C14:1
SCD
C14:0
C16:1
C16:0
ELOVL6
ELOVL1
VLCSFAs
C18:1
SCD
C18:0
Cholesterol synthesis
Free fatty acids
CPT1 CPT2
ACAD ECHS HADH ACAA2
Acyl-CoA
Mitochondrial β-oxidation
Acetyl-CoA
ACOX1 EHHADH ACAA1
Peroxisomal β-oxidation
IF - upregulated
IF - downregulated
Ketone bodies

Figure 6. One-carbon metabolism

(A and B) Heatmap of concentrations (area under the curve [AUC] normalized to total ion count [TIC]) of metabolites related to one-carbon transfer in the serum (hepatic input, A) and liver (B) of the SG and IF-CR groups, expressed as $\log_2$ of the fold-change versus the AL group. (DMG: dimethylglycine; Sarc: sarcosine; Met: methionine; GAA: guanidinoacetate; pEtN: phosphoethanolamine; Hcy: homocysteine; CDP-EtN: cytidine diphosphate-ethanolamine; CDP-Cho: cytidine diphosphate-choline; GPC: glycerophosphocholine; SAM: S-adenosylmethionine; SAH: S-adenosylhomocysteine; pCho: phosphorylcholine; Cys: cystathionine; GGC: gamma-glutamylcysteine; GSH: reduced glutathione).

(C) Ratios in liver of methylated phosphatidylcholine (PC) to unmethylated phosphatidylethanolamine (PE), methylated creatine to unmethylated GAA, and SAM to SAH, in the three experimental groups (concentrations in nmol/mg for PC and PE, and AUC normalized to TIC for creatine, GAA, SAM, and SAH, expressed as standardized z-scores).

(D) Liver concentrations of reduced glutathione (GSH, AUC normalized to TIC) and ratios of GSH to GSSG (expressed as standardized z-scores).

(E) Ratios of hepatic pyruvate to lactate (Pyr/Lac, left), pyruvate to malate (Pyr/Mal, middle), and acetoacetate to beta-hydroxybutyrate (AcAc/beta-HB, right), reflecting cytosolic NAD+/NADH, cytosolic NADP+/NADPH, and mitochondrial NAD+/NADH ratios, respectively (AUC normalized to TIC of each compound was divided by that of the other, and expressed as standardized z-scores).

(F) Heatmaps of relative transcript abundance of significantly altered genes (ANOVA FDR <0.05) related to methyl (CH_3) group transfer, PC and PE synthesis, GSH synthesis, and PC and bile acid (BA) export. Expressed as $\log_2$ of the fold-change versus the AL group.

(G) Plot summarizing changes in one-carbon metabolic pathways. In red, metabolites or transcripts upregulated in the SG group. In blue, metabolites or transcripts down regulated in the SG group.

*$p < 0.05$ ANOVA with Tukey post-hoc test.

**$p < 0.01$ ANOVA with Tukey post-hoc test.

of weight or decreased consumption of fat alone, as they were in direct opposition to the changes seen in the IF-CR group, thus indicating a unique effect of the surgical intervention itself. Our transcriptomic data points to a direct link between changes in liver metabolism following surgery and at least some of the observed alterations in plasma levels of one-carbon metabolites. However, the metabolic composition of the portal blood also reflects changes in the metabolism of the organs drained by this blood vessel, including visceral fat, the stomach, intestine, colon, spleen, and pancreas. Intestinal amino acid catabolism in particular is an important determinant of amino acid availability to extraintestinal tissues.[70,71] Glutamine is the major amino acid consumed by enterocytes, as reflected in our data by the relatively low levels of glutamine in the portal blood. However, the intestinal mucosa also utilizes other dietary amino acids, including methionine, serine, and glycine, derived either directly from the diet or from arterial blood supply. The gastrointestinal tract is the direct target of the bariatric surgical intervention, and intestinal metabolic remodeling may therefore underlie the changes in amino acid concentrations, with altered liver metabolism as a downstream effect. Indeed, changes in intestinal methionine and threonine uptake have been observed with high-fat feeding,[72] and marked changes in intestinal handling of dietary glucose and amino acids[73,74] are described following various types of bariatric surgery, due in part to accelerated gastric emptying.

IF-CR resulted in changes primarily related to fatty acid metabolism. Despite lower levels of circulating free LCFAs, their intrahepatic concentrations were either the same or higher than those seen in the two other groups, likely reflecting increased hepatic DNL. The expression of enzymes involved in DNL was indeed dramatically increased compared to SG and AL fed animals, a finding also reported in a recent study of the intermittent fasting response in mice.[7] Similarly, an increase in lipogenic enzymes was observed in white adipose tissue in rats following cycles of stravation and refeeding.[75] Elevated circulating TGs in the IF-CR probably indicate increased hepatic export of fatty acids to peripheral tissues. The apparent increase in lipogenesis is a somewhat surprising consequence of IF. However, it can be seen as a logical outcome of a once-daily intermittent feeding schedule, where a short period of caloric intake is followed by a prolonged fast. An increased capacity for energy storage, in the form of both fat and glycogen, may be developed as an adpatation to this feeding program, enabling utilization of the calories consumed during a short period throughout the day. This adaptation to fasting may also underlie the relative decrease in ketone bodies seen in the IF-CR group, as the 10-h period without food may not have been sufficient to induce ketogenesis in animals accustomed to daily fasting (in contrast to animals habituated to constant access to food). We do note that our conclusion regarding increased lipogenetic flux is limited by an imperfect correlation between mRNA abundance and metabolic flux, as enzyme activities also depend on post-translational modifications and, critically, substrate availability[76]; therefore, definite conclusions regarding the effect of IF-CR on hepatic DNL would require more direct measurement of lipogenesis at different fasting intervals, and quantification with stable isotope techniques. Nevertheless, expression of key enzymes of lipogenesis was increased up to 50-fold in the IF-CR group, strongly suggesting increased activity of this pathway as a result of the intervention.

DNL hinges on a supply of acetyl-CoA and reducing power in the form of NADPH, derived from the pentose phosphate pathway, the citric acid cycle, and serine metabolism.[77] Indeed, marked upregulation of these

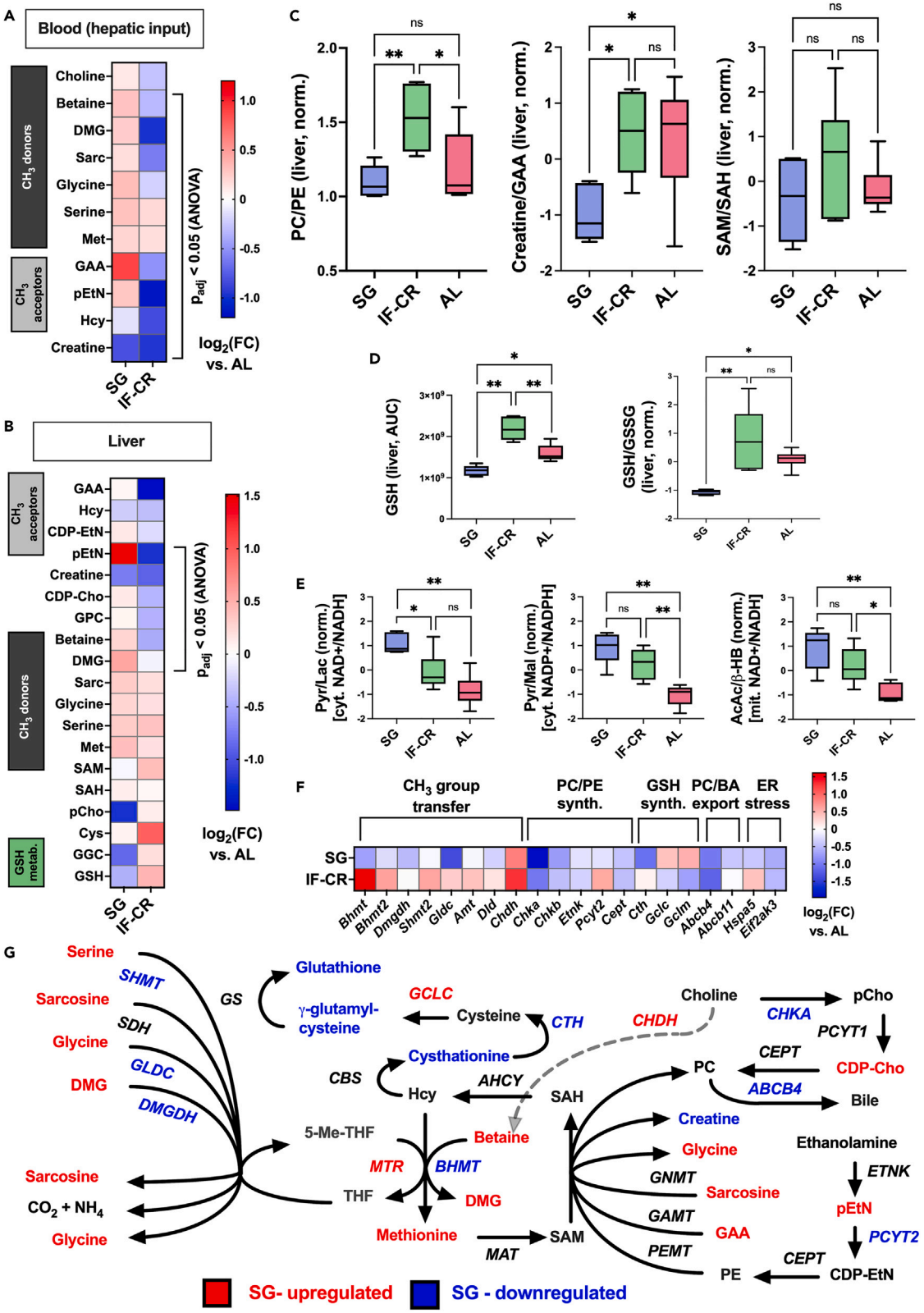
A
Blood (hepatic input)
Choline
Betaine
DMG
Sarc
Glycine
Serine
Met
GAA
pEtN
Hcy
Creatine
CH3 donors
CH3 acceptors
SG
IF-CR
padj < 0.05 (ANOVA)
log2(FC) vs. AL
B
Liver
GAA
Hcy
CDP-EtN
pEtN
Creatine
CDP-Cho
GPC
Betaine
DMG
Sarc
Glycine
Serine
Met
SAM
SAH
pCho
Cys
GGC
GSH
GSH metab.
C
PC/PE (liver, norm.)
Creatine/GAA (liver, norm.)
SAM/SAH (liver, norm.)
ns
SG
IF-CR
AL
D
GSH (liver, AUC)
GSH/GSSG (liver, norm.)
E
Pyr/Lac (norm.) [cyt. NAD+/NADH]
Pyr/Mal (norm.) [cyt. NADP+/NADPH]
AcAc/β-HB (norm.) [mit. NAD+/NADH]
F
CH3 group transfer
PC/PE synth.
GSH synth.
PC/BA export
ER stress
Bhmt
Bhmt2
Dmgdh
Shmt2
Gldc
Amt
Dld
Chdh
Chka
Chkb
Etnk
Pcyt2
Cept
Cth
Gclc
Gclm
Abcb4
Abcb11
Hspa5
Eif2ak3
G
Serine
SHMT
Sarcosine
SDH
Glycine
GLDC
DMG
DMGDH
GS
Glutathione
γ-glutamyl-cysteine
GCLC
Cysteine
CTH
Cysthationine
CBS
Hcy
AHCY
SAH
CHDH
Choline
CHKA
pCho
PCYT1
CDP-Cho
CEPT
PC
ABCB4
Bile
Creatine
Glycine
GNMT
Sarcosine
GAMT
GAA
PEMT
PE
CEPT
CDP-EtN
PCYT2
pEtN
ETNK
Ethanolamine
5-Me-THF
MTR
BHMT
Betaine
THF
DMG
Methionine
MAT
SAM
Sarcosine
CO2 + NH4
Glycine
SG- upregulated
SG - downregulated

Figure 7. Fatty acid metabolism

(A) Heatmap of concentrations of saturated and mono-unsaturated long-chain free fatty acids (SFA/MUFA), poly-unsaturated long-chain free fatty acids (PUFA), and short- and medium-chain free fatty acids (SCFA/MCFA) in the serum (hepatic input) and liver of the SG and IF-CR groups, expressed as log_2 of the fold-change versus the AL group. (* - ANOVA FDR <0.05 in serum or liver).

(B) Serum lipid profile showing increased triglyceride (TG) concentrations in the IF-CR group, as well as decreased high-density lipoprotein (HDL) cholesterol levels in the SG group and no change in low-density lipoprotein (LDL) cholesterol levels.

(C) Serum concentrations (area under the curve [AUC] normalized to total ion count [TIC]) of the major ketone bodies, acetoacetate (AcAc) and beta-hydroxybutyrate (beta-HB), showing a decrease in the IF-CR group.

(E) Heatmaps of relative transcript abundance of significantly altered genes (ANOVA FDR <0.05) in pathways of fatty acid (FA) oxidation and synthesis, glycolysis and gluconeogenesis, pentose phosphate pathway (PPP), and tricarboxylic acid (TCA) cycle, expressed as log_2 of the fold-change versus the AL group, and showing upregulation of FA synthesis in the IF-CR group.

(F) Liver concentrations of glycolytic/gluconeogenic intermediates (AUC normalized to TIC, expressed as standardized z-scores) (G6P: glucose 6-phosphate; F6P: fructose 6-phosphate; GA3P: glyceraldehyde 3-phosphate; DHAP: dihydroxyacetone phosphate; PEP: phosphoenol pyruvate; Pyr: pyruvate).

(G) plot summarizing changes in fatty acid metabolism pathways, glycolysis and gluconeogenesis, pentose phosphate pathway, and TCA cycle. In red, metabolites or transcripts upregulated in the IF-CR group. In blue, metabolites or transcripts down regulated in the IF-CR group. In purple, long-chain FAs – downregulated in serum and upregulated in the liver of the IF-CR group.

*$p < 0.05$ ANOVA with Tukey post-hoc test.

**$p < 0.01$ ANOVA with Tukey post-hoc test.

pathways at the transcriptomic level was observed. Likewise, TG export relies on the liver's ability to synthesize sufficient PC, either directly from dietary choline, or via the methylation of PE, with SAM serving as the methyl donor. Indeed, the ratio of PC to PE was increased in the IF-CR group compared to both other experimental groups. Increased demand for PC may account for the upregulation of enzymes related to methyl group transfer and regeneration of SAM, and the relatively depleted levels of methyl group donors, primarily betaine, seen following IF-CR, in direct opposition to the effect of SG on these pathways.

In addition to the effects on fatty acid metabolism, IF-CR also showed an effect on glucose metabolism, with marked upregulation of genes involved in glycolysis and gluconeogenesis, the pentose phosphate pathway, and the tricarboxylic acid cycle. Most prominent were an upregulation of glucose-6-phosphate dehydrogenase and of malic enzyme 1, both key enzymes in the generation of cytosolic NADPH, presumably in support of lipogenesis. Although generation of reducing equivalents may indeed underlie the observed increase in glucose-metabolizing enzymes, we are aware that many of these also serve gluconeogenesis, which is likely to be predominant after prolonged fasting.

To conclude, our study highlights the disparate metabolic effects of different weight-loss interventions. Overall, although IF-CR resulted in changes across multiple central metabolic pathways, the effects of SG concentrated on one-carbon metabolic pathways. We highlight a unique effect of SG on hepatic one-carbon metabolism and redox balance, which has not been hitherto described, and, intriguingly, find that the metabolic profile established in the liver following SG is similar to that recently described with inhibition of MAT1A,[44] pointing to a potential therapeutic target which may mimic the beneficial effect of surgery on the liver, and through the liver on whole body metabolism. Moreover, the increase in one-carbon donors following surgery may in part mediate the effects on the immune system described following this intervention.

Limitations of the study

The main strength of our study is in the combined transcriptomic and metabolomic analysis, and in the simultaneous examination of the portal and aortic blood pools. However, absent stable isotope tracing studies, we are unable to definitively conclude whether observed alterations in metabolite levels are because of changes in intake or absorption, endogenous synthesis, or consumption. Also, as noted above, mRNA abundances are an imperfect surrogate for metabolic flux. However, the combined data provides strong circumstantial evidence in many cases and allows us to draw conclusions which may be validated by future, directed tracing studies. For example, serum levels of glycine were highest in the SG group, and significantly higher in the portal compared to aortic blood in the AL and IF-CR groups, coinciding with decreased expression of glycine catabolic enzymes in the liver post-SG. We can thus conclude that the increased levels of glycine seen post-SG are likely because of decreased hepatic consumption of this metabolite.

The comparison of two weight loss interventions with an AL-fed control group allowed us to separate the effects of each intervention from the effects of weight loss in general. The groups were compared following an identical period of fasting, reducing the confounding effects of different feeding times on the observed

results. A possible limitation of our study is that sham surgery was not performed in the AL group. The decision not to perform a sham intervention in this group was related to our primary objective of identifying metabolic alterations following equivalent weight loss in SG and IF-CR compared with no intervention at all, including the transient weight-loss induced by the sham surgery. The changes identified could theoretically be attributed to the surgery itself. However, we note that there were few changes in gene expression and metabolite abundance common to the IF-CR and SG groups which could therefore be attributed solely to the effects of laparotomy or anesthesia performed over a month earlier. A further limitation is that we are unable to establish a mechanistic link between the interventions and the observed metabolic and transcriptomic changes, or between the observed changes and the clinical benefit associated with these interventions.

STAR★METHODS

Detailed methods are provided in the online version of this paper and include the following:

- KEY RESOURCES TABLE
- RESOURCE AVAILABILITY
  - Lead contact
  - Materials availability
  - Data and code availability
- EXPERIMENTAL MODEL AND STUDY PARTICIPANT DETAILS
  - Rats
  - Experimental model details
  - Details of surgical interventions
  - Tissue collection
- METHOD DETAILS
  - Sample preparation for mass spectrometry
  - Analysis of metabolites by mass spectrometry
  - RNA sequencing analysis
  - Analysis of phospholipids, glycogen, cholesterol, and triglycerides
- QUANTIFICATION AND STATISTICAL ANALYSIS

SUPPLEMENTAL INFORMATION

Supplemental information can be found online at https://doi.org/10.1016/j.isci.2023.107046.

ACKNOWLEDGMENTS

This project was financially supported by the Israel Science Foundation (967/19) and the European Research Council (StG 803526) and by a grant from the KAMLA Research Fund of the Hebrew University of Jerusalem and Hadassah Medical Center. We would like to thank and acknowledge the contributions of Dr. Idit Shiff and Dr. Abed Nassereddin of the Genomic Applications Laboratory in the Core Research Facility of the Faculty of Medicine, and of Dr. Yuval Nevo and Inbar Plaschkes of the I-CORE Bioinformatics Unit, of the Hebrew University of Jerusalem and Hadassah Medical Center, for their assistance in RNA sequencing experiments and analysis, respectively. We would also like to thank Dr. Gilad Haran for critical discussions and reading of the manuscript. The graphical abstract was created with the use of BioRender.com.

AUTHOR CONTRIBUTIONS

A.H., M.B., R.B.H.S., and S.W.Z. designed the experiments. E.G. assisted in experimental design. A.H., M.B., D.K., S.W.Z., R.B.H.S., and D.B.Z. carried out the animal studies. A.H., M.B., D.K., L.H., H.I., S.W.Z., R.B.H.S., and D.B.Z. participated in sample collection and analysis. BA, IA, and EG conducted the metabolomic analysis. A.H. and D.B.Z. contributed to the final manuscript.

DECLARATION OF INTERESTS

The authors declare no competing interests.

INCLUSION AND DIVERSITY

We support inclusive, diverse, and equitable conduct of research.

Received: November 9, 2022
Revised: March 24, 2023
Accepted: June 1, 2023
Published: June 7, 2023

REFERENCES

1. GBD 2015 Obesity Collaborators, Afshin, A., Forouzanfar, M.H., Reitsma, M.B., Sur, P., Estep, K., Lee, A., Marczak, L., Mokdad, A.H., Moradi-Lakeh, M., et al. (2017). Health effects of overweight and obesity in 195 countries over 25 years. N. Engl. J. Med. *377*, 13–27. https://doi.org/10.1056/NEJMoa1614362.

2. Heymsfield, S.B., and Wadden, T.A. (2017). Mechanisms, pathophysiology, and management of obesity. N. Engl. J. Med. *376*, 254–266. https://doi.org/10.1056/NEJMra1514009.

3. Aminian, A., Jamal, M., Augustin, T., Corcelles, R., Kirwan, J.P., Schauer, P.R., and Brethauer, S.A. (2015). Failed surgical weight loss does not necessarily mean failed metabolic effects. Diabetes Technol. Therapeut. *17*, 682–684. https://doi.org/10.1089/dia.2015.0064.

4. Aminian, A., Zajichek, A., Tu, C., Wolski, K.E., Brethauer, S.A., Schauer, P.R., Kattan, M.W., and Nissen, S.E. (2020). How much weight loss is required for cardiovascular benefits? Insights from a metabolic surgery matched-cohort study. Ann. Surg. *272*, 639–645. https://doi.org/10.1097/SLA.0000000000004369.

5. Harvie, M.N., Pegington, M., Mattson, M.P., Frystyk, J., Dillon, B., Evans, G., Cuzick, J., Jebb, S.A., Martin, B., Cutler, R.G., et al. (2011). The effects of intermittent or continuous energy restriction on weight loss and metabolic disease risk markers: a randomized trial in young overweight women. Int. J. Obes. *35*, 714–727. https://doi.org/10.1038/ijo.2010.171.

6. Harvie, M., Wright, C., Pegington, M., McMullan, D., Mitchell, E., Martin, B., Cutler, R.G., Evans, G., Whiteside, S., Maudsley, S., et al. (2013). The effect of intermittent energy and carbohydrate restriction v. daily energy restriction on weight loss and metabolic disease risk markers in overweight women. Br. J. Nutr. *110*, 1534–1547. https://doi.org/10.1017/S0007114513000792.

7. Hatchwell, L., Harney, D.J., Cielesh, M., Young, K., Koay, Y.C., O'Sullivan, J.F., and Larance, M. (2020). Multi-omics analysis of the intermittent fasting response in mice identifies an unexpected role for HNF4α. Cell Rep. *30*, 3566–3582.e4. https://doi.org/10.1016/j.celrep.2020.02.051.

8. de Cabo, R., and Mattson, M.P. (2019). Effects of intermittent fasting on health, aging, and disease. N. Engl. J. Med. *381*, 2541–2551. https://doi.org/10.1056/NEJMra1905136.

9. Xu, F., Yu, C., Li, D.-G., Yan, Q., Zhang, S.-X., Yang, X.-D., and Zhang, Z. (2020). The outcomes of bariatric surgery on rheumatoid arthritis disease activity: a prospective cohort study. Sci. Rep. *10*, 3167. https://doi.org/10.1038/s41598-020-59723-8.

10. van Huisstede, A., Rudolphus, A., Castro Cabezas, M., Biter, L.U., van de Geijn, G.-J., Taube, C., Hiemstra, P.S., and Braunstahl, G.-J. (2015). Effect of bariatric surgery on asthma control, lung function and bronchial and systemic inflammation in morbidly obese subjects with asthma. Thorax *70*, 659–667. https://doi.org/10.1136/thoraxjnl-2014-206712.

11. Sipe, L.M., Chaib, M., Korba, E.B., Jo, H., Lovely, M.C., Counts, B.R., Tanveer, U., Holt, J.R., Clements, J.C., John, N.A., et al. (2022). Response to immune checkpoint blockade improved in pre-clinical model of breast cancer after bariatric surgery. Elife *11*, e79143. https://doi.org/10.7554/eLife.79143.

12. Laferrère, B., Reilly, D., Arias, S., Swerdlow, N., Gorroochurn, P., Bawa, B., Bose, M., Teixeira, J., Stevens, R.D., Wenner, B.R., et al. (2011). Differential metabolic impact of gastric bypass surgery versus dietary intervention in obese diabetic subjects despite identical weight loss. Sci. Transl. Med. *3*, 80re2. https://doi.org/10.1126/scitranslmed.3002043.

13. Patti, M.-E., Houten, S.M., Bianco, A.C., Bernier, R., Larsen, P.R., Holst, J.J., Badman, M.K., Maratos-Flier, E., Mun, E.C., Pihlajamaki, J., et al. (2009). Serum bile acids are higher in humans with prior gastric bypass: potential contribution to improved glucose and lipid metabolism. Obes. Silver Spring Md *17*, 1671–1677. https://doi.org/10.1038/oby.2009.102.

14. Furet, J.-P., Kong, L.-C., Tap, J., Poitou, C., Basdevant, A., Bouillot, J.-L., Mariat, D., Corthier, G., Doré, J., Henegar, C., et al. (2010). Differential adaptation of human gut microbiota to bariatric surgery-induced weight loss: links with metabolic and low-grade inflammation markers. Diabetes *59*, 3049–3057. https://doi.org/10.2337/db10-0253.

15. Li, G., Xie, C., Lu, S., Nichols, R.G., Tian, Y., Li, L., Patel, D., Ma, Y., Brocker, C.N., Yan, T., et al. (2017). Intermittent fasting promotes white adipose browning and decreases obesity by shaping the gut microbiota. Cell Metabol. *26*, 672–685.e4. https://doi.org/10.1016/j.cmet.2017.08.019.

16. Stefater, M.A., Sandoval, D.A., Chambers, A.P., Wilson-Pérez, H.E., Hofmann, S.M., Jandacek, R., Tso, P., Woods, S.C., and Seeley, R.J. (2011). Sleeve gastrectomy in rats improves postprandial lipid clearance by reducing intestinal triglyceride secretion. Gastroenterology *141*, 939–949.e1-4. https://doi.org/10.1053/j.gastro.2011.05.008.

17. Yoshino, M., Kayser, B.D., Yoshino, J., Stein, R.I., Reeds, D., Eagon, J.C., Eckhouse, S.R., Watrous, J.D., Jain, M., Knight, R., et al. (2020). Effects of diet versus gastric bypass on metabolic function in diabetes. N. Engl. J. Med. *383*, 721–732. https://doi.org/10.1056/NEJMoa2003697.

18. Liu, D., Huang, Y., Huang, C., Yang, S., Wei, X., Zhang, P., Guo, D., Lin, J., Xu, B., Li, C., et al. (2022). Calorie restriction with or without time-restricted eating in weight loss. N. Engl. J. Med. *386*, 1495–1504. https://doi.org/10.1056/NEJMoa2114833.

19. Abu-Gazala, S., Horwitz, E., Ben-Haroush Schyr, R., Bardugo, A., Israeli, H., Hija, A., Schug, J., Shin, S., Dor, Y., Kaestner, K.H., and Ben-Zvi, D. (2018). Sleeve gastrectomy improves glycemia independent of weight loss by restoring hepatic insulin sensitivity. Diabetes *67*, 1079–1085. https://doi.org/10.2337/db17-1028.

20. Ben-Haroush Schyr, R., Al-Kurd, A., Moalem, B., Permyakova, A., Israeli, H., Bardugo, A., Hefetz, L., Bergel, M., Haran, A., Azar, S., et al. (2021). Sleeve gastrectomy suppresses hepatic glucose production and increases hepatic insulin clearance independent of weight-loss. Diabetes, db210251. https://doi.org/10.2337/db21-0251.

21. Chambers, A.P., Jessen, L., Ryan, K.K., Sisley, S., Wilson-Pérez, H.E., Stefater, M.A., Gaitonde, S.G., Sorrell, J.E., Toure, M., Berger, J., et al. (2011). Weight-independent changes in blood glucose homeostasis after gastric bypass or vertical sleeve gastrectomy in rats. Gastroenterology *141*, 950–958. https://doi.org/10.1053/j.gastro.2011.05.050.

22. Samczuk, P., Ciborowski, M., and Kretowski, A. (2018). Application of metabolomics to study effects of bariatric surgery. J. Diabetes Res. *2018*, 6270875. https://doi.org/10.1155/2018/6270875.

23. Stefater, M.A., Pacheco, J.A., Bullock, K., Pierce, K., Deik, A., Liu, E., Clish, C., and Stylopoulos, N. (2020). Portal venous metabolite profiling after RYGB in male rats highlights changes in gut-liver Axis. J. Endocr. Soc. *4*, bvaa003. https://doi.org/10.1210/jendso/bvaa003.

24. Kim, M., Rho, Y., Park, R., Jung, J., Hwang, G.-S., Seo, Y.K., Seo, J.H., Heo, Y., Ha, T.K., and Ha, E. (2021). Duodenal-jejunal bypass maintains hepatic S-adenosylmethionine/S-homocysteine ratio in diet-induced obese rats. Surg. Obes. Relat. Dis. *17*, 1359–1368. https://doi.org/10.1016/j.soard.2021.02.011.

25. Arora, T., Velagapudi, V., Pournaras, D.J., Welbourn, R., le Roux, C.W., Orešič, M., and Bäckhed, F. (2015). Roux-en-Y gastric bypass surgery induces early plasma metabolomic and lipidomic alterations in humans

associated with diabetes remission. PLoS One *10*, e0126401. https://doi.org/10.1371/journal.pone.0126401.

26. Alves-Bezerra, M., and Cohen, D.E. (2017). Triglyceride metabolism in the liver. Compr. Physiol. *8*, 1–8. https://doi.org/10.1002/cphy.c170012.

27. Friedman, S.L., Neuschwander-Tetri, B.A., Rinella, M., and Sanyal, A.J. (2018). Mechanisms of NAFLD development and therapeutic strategies. Nat. Med. *24*, 908–922. https://doi.org/10.1038/s41591-018-0104-9.

28. Lu, Q., Tian, X., Wu, H., Huang, J., Li, M., Mei, Z., Zhou, L., Xie, H., and Zheng, S. (2021). Metabolic changes of hepatocytes in NAFLD. Front. Physiol. *12*, 710420. https://doi.org/10.3389/fphys.2021.710420.

29. Polyzos, S.A., Kountouras, J., and Mantzoros, C.S. (2019). Obesity and nonalcoholic fatty liver disease: from pathophysiology to therapeutics. Metabolism *92*, 82–97. https://doi.org/10.1016/j.metabol.2018.11.014.

30. Abdul Rahim, M.B.H., Chilloux, J., Martinez-Gili, L., Neves, A.L., Myridakis, A., Gooderham, N., and Dumas, M.-E. (2019). Diet-induced metabolic changes of the human gut microbiome: importance of short-chain fatty acids, methylamines and indoles. Acta Diabetol. *56*, 493–500. https://doi.org/10.1007/s00592-019-01312-x.

31. Agus, A., Planchais, J., and Sokol, H. (2018). Gut microbiota regulation of tryptophan metabolism in health and disease. Cell Host Microbe *23*, 716–724. https://doi.org/10.1016/j.chom.2018.05.003.

32. Stead, L.M., Brosnan, J.T., Brosnan, M.E., Vance, D.E., and Jacobs, R.L. (2006). Is it time to reevaluate methyl balance in humans? Am. J. Clin. Nutr. *83*, 5–10. https://doi.org/10.1093/ajcn/83.1.5.

33. van der Veen, J.N., Kennelly, J.P., Wan, S., Vance, J.E., Vance, D.E., and Jacobs, R.L. (2017). The critical role of phosphatidylcholine and phosphatidylethanolamine metabolism in health and disease. Biochim. Biophys. Acta Biomembr. *1859*, 1558–1572. https://doi.org/10.1016/j.bbamem.2017.04.006.

34. Wagner, M., Choi, S., Panzitt, K., Mamrosh, J.L., Lee, J.M., Zaufel, A., Xiao, R., Wooton-Kee, R., Ståhlman, M., Newgard, C.B., et al. (2016). LRH-1 is a critical determinant of methyl-pool metabolism. Hepatol. Baltim. Md *63*, 95–106. https://doi.org/10.1002/hep.28124.

35. Satapati, S., Kucejova, B., Duarte, J.A.G., Fletcher, J.A., Reynolds, L., Sunny, N.E., He, T., Nair, L.A., Livingston, K.A., Fu, X., et al. (2015). Mitochondrial metabolism mediates oxidative stress and inflammation in fatty liver. J. Clin. Invest. *125*, 4447–4462. https://doi.org/10.1172/JCI82204.

36. Gansemer, E.R., McCommis, K.S., Martino, M., King-McAlpin, A.Q., Potthoff, M.J., Finck, B.N., Taylor, E.B., and Rutkowski, D.T. (2020). NADPH and glutathione redox link TCA cycle activity to endoplasmic reticulum homeostasis. iScience *23*, 101116. https://doi.org/10.1016/j.isci.2020.101116.

37. Reddy, J.K. (2001). III. Peroxisomal β-oxidation, PPARα, and steatohepatitis. Am. J. Physiol. Gastrointest. Liver Physiol. *281*, G1333–G1339. https://doi.org/10.1152/ajpgi.2001.281.6.G1333.

38. Schlaepfer, I.R., and Joshi, M. (2020). CPT1A-mediated fat oxidation, mechanisms, and therapeutic potential. Endocrinology *161*, bqz046. https://doi.org/10.1210/endocr/bqz046.

39. Donaldson, W.E. (1979). Regulation of fatty acid synthesis. Fed. Proc. *38*, 2617–2621.

40. Ghosh, S., Forney, L.A., Wanders, D., Stone, K.P., and Gettys, T.W. (2017). An integrative analysis of tissue-specific transcriptomic and metabolomic responses to short-term dietary methionine restriction in mice. PLoS One *12*, e0177513. https://doi.org/10.1371/journal.pone.0177513.

41. Tamanna, N., Kroeker, K., Braun, K., Banh, S., and Treberg, J.R. (2019). The effect of short-term methionine restriction on glutathione synthetic capacity and antioxidant responses at the whole tissue and mitochondrial level in the rat liver. Exp. Gerontol. *127*, 110712. https://doi.org/10.1016/j.exger.2019.110712.

42. Maddineni, S., Nichenametla, S., Sinha, R., Wilson, R.P., and Richie, J.P. (2013). Methionine restriction affects oxidative stress and glutathione-related redox pathways in the rat. Exp. Biol. Med. *238*, 392–399. https://doi.org/10.1177/1535370213477988.

43. Robinson, J.L., McBreairty, L.E., Randell, E.W., Brunton, J.A., and Bertolo, R.F. (2016). Restriction of dietary methyl donors limits methionine availability and affects the partitioning of dietary methionine for creatine and phosphatidylcholine synthesis in the neonatal piglet. J. Nutr. Biochem. *35*, 81–86. https://doi.org/10.1016/j.jnutbio.2016.07.001.

44. Sáenz de Urturi, D., Buqué, X., Porteiro, B., Folgueira, C., Mora, A., Delgado, T.C., Prieto-Fernández, E., Olaizola, P., Gómez-Santos, B., Apodaka-Biguri, M., et al. (2022). Methionine adenosyltransferase 1a antisense oligonucleotides activate the liver-brown adipose tissue axis preventing obesity and associated hepatosteatosis. Nat. Commun. *13*, 1096. https://doi.org/10.1038/s41467-022-28749-z.

45. Avila, M.A., Corrales, F.J., Ruiz, F., Sánchez-Góngora, E., Mingorance, J., Carretero, M.V., and Mato, I.M. (1998). Specific interaction of methionine adenosyltransferase with free radicals. Biofactors *8*, 27–32. https://doi.org/10.1002/biof.5520080106.

46. Pajares, M.A., Durán, C., Corrales, F., Pliego, M.M., and Mato, J.M. (1992). Modulation of rat liver S-adenosylmethionine synthetase activity by glutathione. J. Biol. Chem. *267*, 17598–17605. https://doi.org/10.1016/S0021-9258(19)37084-X.

47. Corrales, F.J., Pérez-Mato, I., Sánchez Del Pino, M.M., Ruiz, F., Castro, C., García-Trevijano, E.R., Latasa, U., Martínez-Chantar, M.L., Martínez-Cruz, A., Avila, M.A., and Mato, J.M. (2002). Regulation of mammalian liver methionine adenosyltransferase. J. Nutr. *132*, 2377S–2381S. https://doi.org/10.1093/jn/132.8.2377S.

48. Ruiz, F., Corrales, F.J., Miqueo, C., and Mato, J.M. (1998). Nitric oxide inactivates rat hepatic methionine adenosyltransferase in vivo by S-nitrosylation. Hepatology *28*, 1051–1057. https://doi.org/10.1002/hep.510280420.

49. Sledzinski, T., Sledzinski, M., Smolenski, R.T., and Swierczynski, J. (2010). Increased serum nitric oxide concentration after bariatric surgery—a potential mechanism for cardiovascular benefit. Obes. Surg. *20*, 204–210. https://doi.org/10.1007/s11695-009-0041-2.

50. Patle, R., Dubb, S., Alaghband-Zadeh, J., Sherwood, R.A., Tam, F., Frankel, A., Moniz, C., Bueter, M., Vincent, R.P., and le Roux, C.W. (2012). Improved blood pressure, nitric oxide and asymmetric dimethylarginine are independent after bariatric surgery. Ann. Clin. Biochem. *49*, 589–594. https://doi.org/10.1258/acb.2012.012069.

51. Ding, L., and Zhang, J. (2012). Glucagon-like peptide-1 activates endothelial nitric oxide synthase in human umbilical vein endothelial cells. Acta Pharmacol. Sin. *33*, 75–81. https://doi.org/10.1038/aps.2011.149.

52. Barale, C., Buracco, S., Cavalot, F., Frascaroli, C., Guerrasio, A., and Russo, I. (2017). Glucagon-like peptide 1-related peptides increase nitric oxide effects to reduce platelet activation. Thromb. Haemostasis *117*, 1115–1128. https://doi.org/10.1160/TH16-07-0586.

53. Ahrens, M., Ammerpohl, O., von Schönfels, W., Kolarova, J., Bens, S., Itzel, T., Teufel, A., Herrmann, A., Brosch, M., Hinrichsen, H., et al. (2013). DNA methylation analysis in nonalcoholic fatty liver disease suggests distinct disease-specific and remodeling signatures after bariatric surgery. Cell Metabol. *18*, 296–302. https://doi.org/10.1016/j.cmet.2013.07.004.

54. Yang, S., Zhu, H., Li, Y., Lin, H., Gabrielson, K., Trush, M.A., and Diehl, A.M. (2000). Mitochondrial adaptations to obesity-related oxidant stress. Arch. Biochem. Biophys. *378*, 259–268. https://doi.org/10.1006/abbi.2000.1829.

55. Garcia, M.C., Amankwa-Sakyi, M., and Flynn, T.J. (2011). Cellular glutathione in fatty liver in vitro models. Toxicol. Vitro *25*, 1501–1506. https://doi.org/10.1016/j.tiv.2011.05.011.

56. Merry, T.L., Tran, M., Dodd, G.T., Mangiafico, S.P., Wiede, F., Kaur, S., McLean, C.L., Andrikopoulos, S., and Tiganis, T. (2016). Hepatocyte glutathione peroxidase-1 deficiency improves hepatic glucose metabolism and decreases steatohepatitis in mice. Diabetologia *59*, 2632–2644. https://doi.org/10.1007/s00125-016-4084-3.

57. Nussbaum, J.M., Liu, L.J., Hasan, S.A., Schaub, M., McClendon, A., Stainier, D.Y.R., and Sakaguchi, T.F. (2013). Homeostatic generation of reactive oxygen species protects the zebrafish liver from steatosis.

Hepatol. Baltim. Md *58*, 1326–1338. https://doi.org/10.1002/hep.26551.

58. Haque, J.A., McMahan, R.S., Campbell, J.S., Shimizu-Albergine, M., Wilson, A.M., Botta, D., Bammler, T.K., Beyer, R.P., Montine, T.J., Yeh, M.M., et al. (2010). Attenuated progression of diet-induced steatohepatitis in glutathione-deficient mice. Lab. Invest. *90*, 1704–1717. https://doi.org/10.1038/labinvest.2010.112.

59. Laursen, T.L., Hagemann, C.A., Wei, C., Kazankov, K., Thomsen, K.L., Knop, F.K., and Grønbæk, H. (2019). Bariatric surgery in patients with non-alcoholic fatty liver disease - from pathophysiology to clinical effects. World J. Hepatol. *11*, 138–149. https://doi.org/10.4254/wjh.v11.i2.138.

60. da Silva, V.R.G., Moreira, E.a.M., Wilhelm-Filho, D., de Miranda, J.X., Benincá, J.P., Vigil, S.V.G., Moratelli, A.M.B., Garlet, T.R., de Souza Meirelles, M.S., Vannucchi, H., and Fröde, T.S. (2012). Proinflammatory and oxidative stress markers in patients submitted to Roux-en-Y gastric bypass after 1 year of follow-up. Eur. J. Clin. Nutr. *66*, 891–899. https://doi.org/10.1038/ejcn.2012.17.

61. Horn, R.C., Gelatti, G.T., Mori, N.C., Tissiani, A.C., Mayer, M.S., Pereira, E.A., Ross, M., Moreira, P.R., Bortolotto, J.W., and Felippin, T. (2017). Obesity, bariatric surgery and oxidative stress. Rev. Assoc. Med. Bras. *63*, 229–235. https://doi.org/10.1590/1806-9282.63.03.229.

62. Holt, E.W., DeMartini, S., and Davern, T.J. (2015). Acute liver failure due to acetaminophen poisoning in patients with prior weight loss surgery: a case series. J. Clin. Gastroenterol. *49*, 790–793. https://doi.org/10.1097/MCG.0000000000000278.

63. Roy, D.G., Chen, J., Mamane, V., Ma, E.H., Muhire, B.M., Sheldon, R.D., Shorstova, T., Koning, R., Johnson, R.M., Esaulova, E., et al. (2020). Methionine metabolism shapes T helper cell responses through regulation of epigenetic reprogramming. Cell Metabol. *31*, 250–266.e9. https://doi.org/10.1016/j.cmet.2020.01.006.

64. Zhao, T., and Lum, J.J. (2022). Methionine cycle-dependent regulation of T cells in cancer immunity. Front. Oncol. *12*, 969563.

65. Dorado, E., Suso, J.P., Cañas, C.A., Bonilla-Abadía, F., Ospina, F.E., Agualimpia, A., Echeverri, A.F., Castaño, G.L., Martínez, J.D., Tobón, G.J., et al. (2016). Immunologic changes after bariatric surgery: is it A trigger for systemic autoimmune diseases? Surg. Obes. Relat. Dis. *12*, S204. https://doi.org/10.1016/j.soard.2016.08.354.

66. Anna Karin, H., Erik, S., Tim, S., Lars, F., Erik, N., and Jan, H. (2022). The impact of bariatric surgery on disease activity and progression of multiple sclerosis: a nationwide matched cohort study. Mult. Scler. *28*, 2099–2105. https://doi.org/10.1177/13524585221107095.

67. Alves, A., Bassot, A., Bulteau, A.-L., Pirola, L., and Morio, B. (2019). Glycine metabolism and its alterations in obesity and metabolic diseases. Nutrients *11*, 1356. https://doi.org/10.3390/nu11061356.

68. White, P.J., Lapworth, A.L., McGarrah, R.W., Kwee, L.C., Crown, S.B., Ilkayeva, O., An, J., Carson, M.W., Christopher, B.A., Ball, J.R., et al. (2020). Muscle-liver trafficking of BCAA-derived nitrogen underlies obesity-related Glycine depletion. Cell Rep. *33*, 108375. https://doi.org/10.1016/j.celrep.2020.108375.

69. Pacana, T., Cazanave, S., Verdianelli, A., Patel, V., Min, H.-K., Mirshahi, F., Quinlivan, E., and Sanyal, A.J. (2015). Dysregulated hepatic methionine metabolism drives homocysteine elevation in diet-induced nonalcoholic fatty liver disease. PLoS One *10*, e0136822. https://doi.org/10.1371/journal.pone.0136822.

70. Wu, G. (1998). Intestinal mucosal amino acid catabolism. J. Nutr. *128*, 1249–1252. https://doi.org/10.1093/jn/128.8.1249.

71. Bauchart-Thevret, C., Stoll, B., and Burrin, D.G. (2009). Intestinal metabolism of sulfur amino acids. Nutr. Res. Rev. *22*, 175–187. https://doi.org/10.1017/S0954422409990138.

72. Poupin, N., Tremblay-Franco, M., Amiel, A., Canlet, C., Rémond, D., Debrauwer, L., Dardevet, D., Thiele, I., Aurich, M.K., Jourdan, F., et al. (2019). Arterio-venous metabolomics exploration reveals major changes across liver and intestine in the obese Yucatan minipig. Sci. Rep. *9*, 12527. https://doi.org/10.1038/s41598-019-48997-2.

73. Cavin, J.-B., Couvelard, A., Lebtahi, R., Ducroc, R., Arapis, K., Voitellier, E., Cluzeaud, F., Gillard, L., Hourseau, M., Mikail, N., et al. (2016). Differences in alimentary glucose absorption and intestinal disposal of blood glucose after roux-en-Y gastric bypass vs sleeve gastrectomy. Gastroenterology *150*, 454–464.e9. https://doi.org/10.1053/j.gastro.2015.10.009.

74. Svane, M.S., Bojsen-Møller, K.N., Martinussen, C., Dirksen, C., Madsen, J.L., Reitelseder, S., Holm, L., Rehfeld, J.F., Kristiansen, V.B., van Hall, G., et al. (2019). Postprandial nutrient handling and gastrointestinal hormone secretion after roux-en-Y gastric bypass vs sleeve gastrectomy. Gastroenterology *156*, 1627–1641.e1. https://doi.org/10.1053/j.gastro.2019.01.262.

75. Karbowska, J., Kochan, Z., and Swierczynski, J. (2001). Increase of lipogenic enzyme mRNA levels in rat white adipose tissue after multiple cycles of starvation-refeeding. Metabolism *50*, 734–738. https://doi.org/10.1053/meta.2001.23309.

76. Hoppe, A. (2012). What mRNA abundances can tell us about metabolism. Metabolites *2*, 614–631. https://doi.org/10.3390/metabo2030614.

77. Jin, E.S., Lee, M.H., Murphy, R.E., and Malloy, C.R. (2018). Pentose phosphate pathway activity parallels lipogenesis but not antioxidant processes in rat liver. Am. J. Physiol. Endocrinol. Metab. *314*, E543–E551. https://doi.org/10.1152/ajpendo.00342.2017.

78. Bruinsma, B.G., Uygun, K., Yarmush, M.L., and Saeidi, N. (2015). Surgical models of Roux-en-Y gastric bypass surgery and sleeve gastrectomy in rats and mice. Nat. Protoc. *10*, 495–507. https://doi.org/10.1038/nprot.2015.027.

79. Eipel, C., Abshagen, K., and Vollmar, B. (2010). Regulation of hepatic blood flow: the hepatic arterial buffer response revisited. World J. Gastroenterol. *16*, 6046–6057. https://doi.org/10.3748/wjg.v16.i48.6046.

80. Mackay, G.M., Zheng, L., van den Broek, N.J.F., and Gottlieb, E. (2015). Analysis of cell metabolism using LC-MS and isotope tracers. Methods Enzymol. *561*, 171–196. https://doi.org/10.1016/bs.mie.2015.05.016.

81. Martin, M. (2011). Cutadapt removes adapter sequences from high-throughput sequencing reads. EMBnet. j. *17*, 10–12. https://doi.org/10.14806/ej.17.1.200.

82. TopHat2: Accurate Alignment of Transcriptomes in the Presence of Insertions, Deletions and Gene Fusions | Genome Biology | Full Text. https://genomebiology.biomedcentral.com/articles/10.1186/gb-2013-14-4-r36.

83. Anders, S., Pyl, P.T., and Huber, W. (2015). HTSeq—a Python framework to work with high-throughput sequencing data. Bioinformatics *31*, 166–169. https://doi.org/10.1093/bioinformatics/btu638.

84. Pang, Z., Chong, J., Zhou, G., de Lima Morais, D.A., Chang, L., Barrette, M., Gauthier, C., Jacques, P.É., Li, S., and Xia, J. (2021). MetaboAnalyst 5.0: narrowing the gap between raw spectra and functional insights. Nucleic Acids Res. *49*, W388–W396. https://doi.org/10.1093/nar/gkab382.

85. Controlling the False Discovery Rate: A Practical and Powerful Approach to Multiple Testing - Benjamini - 1995 - Journal of the Royal Statistical Society: Series B (Methodological) - Wiley Online Library. https://rss.onlinelibrary.wiley.com/doi/10.1111/j.2517-6161.1995.tb02031.x.

86. Moderated Estimation of Fold Change and Dispersion for RNA-Seq Data with DESeq2 | Genome Biology | Full Text. https://genomebiology.biomedcentral.com/articles/10.1186/s13059-014-0550-8.

87. Ruebel, M.L., Piccolo, B.D., Mercer, K.E., Pack, L., Moutos, D., Shankar, K., and Andres, A. (2019). Obesity leads to distinct metabolomic signatures in follicular fluid of women undergoing in vitro fertilization. Am. J. Physiol. Endocrinol. Metab. *316*, E383–E396. https://doi.org/10.1152/ajpendo.00401.2018.

STAR★METHODS

KEY RESOURCES TABLE

REAGENT or RESOURCE	SOURCE	IDENTIFIER
Chemicals, peptides, and recombinant proteins		
Isoflurane, USP 100% (Terrell)	Piramal Critical Care, Inc.	NDC code: 66794-017-10
Meloxicam 5 mg/ml (Loxicom)	Norbrook	ANADA code: #200-491
D-(+)-Glucose	Sigma-Aldrich/Merck	Cat#16325
UltraPure DNase/RNase-Free Water	Bio-Lab Ltd.	Cat#1249301
Povidone iodine 10% (Polydine)	Dr. Fischer, Israel	License #131.96.23410
Pentobarbital sodium 200 mg/ml (Pental)	CTS Chemical Industries, Ltd.	077-29-91952-00
Methanol LC-MS	J.T. Baker	Cat#9830
Acetonitrile LC-MS	J.T. Baker	Cat#9829
Isotope-labeled internal standards (glucose, glutamine, pyruvate, glutamate, lactate)	Cambridge Isotope Laboratories	Cat#CLM-1396-5, CLM-1822-H-PK, CLM-2440-1, CLM-3949-0.25, CLM-1579-0.5
Ethanol	J.T. Baker	Cat#8025
Isopropyl alcohol	Gadot group, Israel	Cat#830111370
Mayer's hematoxylin solution	Sigma-Aldrich/Merck	Cat#MHS32-1L
Eosin solution	Sigma-Aldrich/Merck	Cat#HT110116-500ML
Ammonium carbonate	Fluka	Cat#74415-250G
Critical commercial assays		
TRI Reagent	Sigma-Aldrich/Merck	Cat#93289
Pierce BCA protein assay kit	Thermo scientific	Cat#23227
Phosphatidylcholine assay kit	Abcam	Cat#ab83377
Phosphatidylethanolamine assay kit	Abcam	Cat#ab241005
Glycogen assay kit	Abcam	Cat#ab65620
PAS staining kit	Merck	Cat#101646
Alcian blue solution	Merck	Cat#101647
Cobas C111 Triglycerides	Roche diagnostics	Cat#04657594190
Cobas C111 LDL-C Gen3	Roche diagnostics	Cat#07005806190
Cobas C111 HDL-C Gen4	Roche diagnostics	Cat#07528604190
Cobas C111 Cholesterin	Roche diagnostics	Cat#04718917190
RNA ScreenTape kit	Agilent Technologies	Cat#5067-5576
D1000 ScreenTape kit	Agilent Technologies	Cat#5067-5582
Qubit® RNA HS Assay kit	Invitrogen	Cat#Q32852
Qubit® DNA HS Assay kit	Invitrogen	Cat#32854
KAPA Stranded mRNA-Seq Kit	Kapa Biosystems	Cat#KK8421
NextSeq 500/550 High Output v2 kit (75 cycles) cartridge	Illumina	Cat#FC-404-1005
Deposited data		
RNA sequencing and metabolomics data	Mendeley Data	https://doi.org/10.17632/fy7zbmxfjk.1
Experimental models: Organisms/strains		
Hsd:Sprague Dawley SD male rats	Envigo Israel	Hsd:Sprague Dawley SD
Software and algorithms		
Thermo Xcalibur	Thermo Fisher Scientific	Version 4.1
TraceFinder	Thermo Fisher Scientific	Version 4.1

(*Continued on next page*)

Continued

REAGENT or RESOURCE	SOURCE	IDENTIFIER
Compound Discoverer	Thermo Fisher Scientific	Version 3.0
FastQC	Babraham Bioinformatics	Version 0.11.9
Cutadapt	NBIS	Version 3.1
TopHat	Johns Hopkins University	Version 2.1.1
DESeq2	Bioconductor	Version 3.12
Matlab	MathWorks	Version R2020a
MetaboAnalyst	GenomeCanada	Version 4.1.3
R	R Project	Version 4.0.1
Other		
45% kcal fat diet	Envigo/Inotiv	TD.08811
Endo GIA surgical stapler	Covidien	Cat#EGIA60AMT
Accu-Chek Performa glucometer	Roche Diabetes Care Ltd.	Cat#06987788039
Accu-Chek Performa test strips	Roche Diabetes Care Ltd.	Cat#06454011018
Coated Vicryl absorable suture	Ethicon	Cat#W9501
Scalp vein set, 23G X 3/4"	Anhui Hongyu Wuzhou, Ltd.	Cat#OMG-W-01-055B
MiniCollect lithium heparin collection tube	Greiner Bio-One	Cat#450535
CK14 soft tissue homogenizing tubes	Bertin Corp.	Cat#P000933-LYSK0-A
Precellys tubes	Bertin Technologies	Cat#P000945-LYSK0-A

RESOURCE AVAILABILITY

Lead contact

Further information and requests for resources and reagents should be directed to and will be fulfilled by the lead contact, Arnon Haran (arnon@hadassah.org.il).

Materials availability

This study did not generate new unique reagents.

Data and code availability

- RNA sequencing and metabolomics data have been deposited at Mendeley and are publicly available as of the date of publication. DOIs are listed in the key resources table.
- This paper does not report original code.
- Any additional information required to reanalyze the data reported in this paper is available from the lead contact upon request.

EXPERIMENTAL MODEL AND STUDY PARTICIPANT DETAILS

Rats

All experiments were approved by the institutional animal care and use committee. Five-week-old male Hsd:Sprague-Dawley rats purchased from Envigo (Ness-Ziona, Israel) were used for the studies. Animals were housed in pairs and were maintained on a 12-hour light, 12-hour dark cycle in a temperature-controlled room (22 $\pm$ 2°C).

Experimental model details

The animals were fed a HFHSD (Envigo TD.08811) for a total of 12 weeks, during which they were divided into three experimental groups (see Figure 1A). One group (8 rats) underwent SG following seven weeks of high-fat, high-sucrose feeding, a second group (6 rats) underwent sham operation at the same time and then underwent an IF-CR diet with the goal of reaching the same end-experimental weight as the SG-treated rats, and a third group (6 rats) was allowed to consume food freely and did not undergo any intervention (*ad libitum* [AL]). During caloric restriction, food was provided once daily in the evening. The

amount of food was initially restricted to 10 grams/animal/day to and was then gradually increased up to 20 grams/animal/day.

Oral glucose tolerance tests were carried out in the SG and IF-CR groups at week 10. Oral gavage of 2 g/kg glucose was administered following an overnight fast, and serum glucose was determined using an Accu-Chek Performa glucometer (Roche Diagnostics Ltd.) at intervals of 15-30 minutes up to 120 minutes post-gavage. Random, non-fasting measurements of serum glucose were also carried out in all experimental groups once to twice weekly.

Details of surgical interventions

Rats were fasted for the 12 hours before and for the first 24 hours after surgical interventions and were then maintained on a liquid diet for a further 72 hours, following which the preoperative diet was returned. Surgery was performed under inhalational anesthesia (isoflurane) and post-operative analgesia (meloxicam) was administered daily for the 5 days following surgery.

SG was performed with the use of a Covidien Endo GIA surgical stapler. A midline incision was made, and the stapler was positioned to achieve a removal of 70-80% of the stomach, following previously described protocols.[78] For sham operations, a midline incision was followed by manual manipulation of the stomach only.

Tissue collection

At week 12, five weeks after surgery in the interventional groups, and following a 10-hour overnight fast, blood samples from the portal vein and the aorta were obtained, as well as tissue samples from the liver. For the AL and SG groups, food was removed from the cages at 10 hours prior to sacrifice; for the IF-CR group, once-daily feeding was provided at 10 hours prior to sacrifice, and any remaining food was then removed. Anesthesia was achieved with intraperitoneal phenobarbital. All samples were immediately frozen in liquid nitrogen and then stored at -80°C until their analysis.

METHOD DETAILS

All animals in the IF-CR and AL groups were included in the final analysis. In the SG groups, two animals died due to surgical complications and one animal died prior to obtaining blood and tissue samples due to anesthetic complications. Therefore, data from only five animals in this group were included in the final analysis.

Sample preparation for mass spectrometry

Metabolomic analysis of the hepatic input and metabolomic and transcriptomic analysis of the liver itself were performed in the three experimental groups. Portal and aortic blood samples were analyzed separately, and the hepatic input was then defined as their combination in a 4:1 ratio.[79]

Metabolite extraction was performed as follows: frozen rat plasma and liver samples were thawed on ice. 10 μL of each plasma sample were diluted in 190 μL of precooled (-20° C) methanol:acetonitrile 3:1 extraction solution and vortexed for 10 minutes at 4°C to extract metabolites. The extraction solution was prepared with isotope-labeled internal standards (20 μM $^{13}C_6$-glucose, 4 μM $^{13}C_5$-glutamine, 2 μM $^{13}C_3$-pyruvate, 10 μM $^{13}C_5$-glutamate, 10 μM $^{13}C_3$-alanine, and 10 μM $^{13}C_3$-lactate; Cambridge Isotope Laboratories). Vortexed plasma samples were centrifuged at 4°C for 15 minutes at 16,000g to pellet proteins. The supernatant was then transferred into high-performance liquid chromatography (HPLC) glass vials containing a glass insert and stored at -80°C until liquid chromatography-mass spectrometry (LC-MS) analysis. Frozen liver samples weighing 30 mg each were suspended in CK14 soft tissue homogenizing tubes (Bertin Corp., Rockville, MD, USA) containing 1,000 μL precooled (-20° C) methanol:acetonitrile:water 5:3:2 extraction solution and 1.4 mm ceramic beads. The extraction solution was prepared with the same isotope-labeled internal standards as specified above for plasma samples. Samples were homogenized using a Precellys 24 tissue homogenizer (Bertin Technologies, Montigny-le-Bretonneux, France) cooled to 4° C (3 X 20 seconds at 6000 rpm, with a 30 second gap between each of the three cycles). Homogenized extracts were centrifuged in the Precellys tubes at 18,000 g for 15 min at 4°C, and supernatants were collected in microcentrifuge tubes and centrifuged again at 18,000 g for 10 min at 4°C. The supernatants were then transferred to glass HPLC vials and kept at -80 °C prior to LC-MS analysis.

Analysis of metabolites by mass spectrometry

LC-MS analysis was conducted as described previously[80] with minor adaptations. Briefly, a Thermo Ultimate 3000 HPLC system coupled to a Q-Exactive Orbitrap Mass Spectrometer (Thermo Fisher Scientific) was used with a resolution of 35,000 at 200 mass/charge ratio (m/z), electrospray ionization, and polarity switching mode to enable both positive and negative ions across a mass range of 67 to 1000 m/z. HPLC setup consisted of a ZIC-pHILIC column (SeQuant; 150 mm × 2.1 mm, 5 μm; Merck) with a ZIC-pHILIC guard column (SeQuant; 20 mm ×2.1 mm). 5 μl of rat plasma or liver extract were injected, and the compounds were separated with mobile phase gradient of 15 min, starting at 20% aqueous (20 mM ammonium carbonate adjusted to pH 9.2 with 0.1% of 25% ammonium hydroxide) and 80% organic (acetonitrile) and terminated with 20% acetonitrile. Flow rate and column temperature were maintained at 0.2 ml/min and 45°C, respectively, for a total run time of 27 min. All metabolites were detected using mass accuracy below 5 ppm. Thermo Xcalibur was used for data acquisition. Quality control standards containing only extraction mix and processed as described above, as well as a quality control mix of all samples, were used to assess for technical variability. Using the software TraceFinder 4.1 (Thermo Fisher Scientific), raw data were extracted and matched to a reference library built by running commercial standards for all detected metabolites, based on expected retention time and mass. For data normalization, raw data files were processed with Compound Discoverer 3.0 to obtain total measurable ion peak intensities for each sample. Automatic identification was followed by manual curation to ensure accuracy. Peaks were quantified using the area under the curve and normalized to the total ion count (TIC) measured for each sample. Fatty acids measured were non-esterified, free fatty acids.

RNA sequencing analysis

RNA was isolated from liver tissue using a TRI reagent-based protocol. cDNA libraries were prepared using 1000 ng of RNA per sample and following poly(A) enrichment, using the KAPA Stranded mRNA-Seq kit (Kapa Biosystems). RNA and DNA quantity and quality were assessed using an Agilent TapeStation system (Agilent Technologies, Santa Clara, California) and a Qubit fluorometer (Invitrogen, Carlsbad, California), respectively. RNA integrity numbers were >8.2 for all samples. Libraries were normalized and pooled together. Pooled samples were then loaded on the Illumina NextSeq 500 sequencing system, with 75 cycles and single-read sequencing conditions. Raw reads were inspected for quality issues with FastQC. Following that, the reads were quality-trimmed with Cutadapt[81], using a quality threshold of 32 for both ends. The processed reads were aligned to the rat transcriptome and genome with TopHat,[82] allowing for five mismatches. Quantification was done with HTseq-count.[83]

Analysis of phospholipids, glycogen, cholesterol, and triglycerides

Phosphatidylcholine (PC), phosphatidylethanolamine (PE), and glycogen content in liver tissue were measured using Abcam colorimetric/fluorimetric assays (ab83377, ab241005, and ab65620, respectively), following the manufacturer's instructions. Serum triglycerides (TG), low-density lipoprotein (LDL) cholesterol, and high-density lipoprotein (HDL) cholesterol, were determined using a Cobas c111 analyzer (Roche Diagnostics Ltd.).

QUANTIFICATION AND STATISTICAL ANALYSIS

All metabolomic statistical analyses were carried out using MetaboAnalyst.[84] One-way analysis of variance (ANOVA) was used to recognize individual metabolites or genes whose concentrations or expression, respectively, were significantly altered between the experimental groups. Correction for multiple comparisons was carried out using the Benjamini-Hochberg procedure[85] with a false discovery rate (FDR) or adjusted p-value cutoff of 0.05. ANOVA post-hoc analyses were performed using Fisher's least significant differences (LSD) procedure or, where noted, Tukey's honestly significant difference (HSD) test.

Differential gene expression analysis was carried out using DESeq2[86] and Matlab. Low expression genes were filtered out prior to analysis based on a threshold of average expression of less than 1 copy per million across samples. The significance threshold was set as an adjusted p-value of <0.05, following correction for multiple comparisons carried out using the Benjamini-Hochberg procedure.[85]

Multivariate dimensionality reduction using partial least squares-discriminant analysis (PLS-DA) was used to identify groups of metabolites discriminating between the experimental groups. Metabolites were defined as belonging to components one, two, or neither, based on their variable importance in projection

(VIP) score for that component being above 1.0 (an accepted threshold[87]) and greater than the VIP score for the other component. Pathway enrichment of each component was then carried out using the small molecule pathway database (SBPDB).

For differentially expressed genes, enrichment analysis by Kyoto Encyclopedia of Genes and Genomes (KEGG) pathway was performed separately for upregulated and downregulated genes in each of the intervention groups (i.e., SG and IF-CR); these were defined as genes identified by ANOVA and post-hoc analysis as significantly altered against at least one of the other experimental groups, and with either a negative or positive fold-change compared to both other.